NASA TECHNICAL NOTE

NASA TN D-5243

AN ANALYTICAL STUDY OF LUNAR SURFACE SHAPE AND SIZE FROM LUNAR ORBITER MISSION I PHOTOGRAPHS

by Ruben L. Jones

Langley Research Center
Langley Station, Hampton, Va.

NATIONAL AERONAUTICS AND SPACE ADMINISTRATION • WASHINGTON, D. C. • JUNE 1969

AN ANALYTICAL STUDY OF LUNAR SURFACE SHAPE AND SIZE FROM LUNAR ORBITER MISSION I PHOTOGRAPHS

By Ruben L. Jones

Langley Research Center
Langley Station, Hampton, Va.

NATIONAL AERONAUTICS AND SPACE ADMINISTRATION

For sale by the Clearinghouse for Federal Scientific and Technical Information
Springfield, Virginia 22151 – CFSTI price $3.00

AN ANALYTICAL STUDY OF LUNAR SURFACE SHAPE AND SIZE FROM LUNAR ORBITER MISSION I PHOTOGRAPHS

By Ruben L. Jones
Langley Research Center

SUMMARY

A study of the Lunar Orbiter photographs is being conducted which, when complete, should yield a very precise estimate of the lunar size and shape and contribute significantly to the establishment of an accurate selenodetic system. This paper is a preliminary report on results obtained from mission I photography, in addition to a discussion of the photogrammetric reduction techniques being utilized and the established film reading practices.

Selenographic coordinates of many distinct lunar features were calculated with an expected uncertainty of ±200 m by a digital computer program using film readings as input and are represented by computer-produced contour charts of the lunar sites. These machine-produced charts are found to be in agreement with isolated radii obtained independently with the use of the Lunar Orbiter V/H sensor (which had an expected uncertainty of ±700 m) and from a qualitative point of view are found to agree with Ranger tracking data.

The arithmetic mean of approximately 2000 radii distributed between ±45° longitude and ±5° latitude was found to be 1735.7 km, whereas the two equatorial semiaxes were found to be 1736.6 km and 1734.2 km at 0° and 90° longitude, respectively. Thus, the results of this study suggest that the currently accepted value of the mean lunar radius of 1738 km is in error.

INTRODUCTION

The geometric size and shape of the moon (lunar figure) has been the object of scientific studies involving many different techniques all of which have relied on earth-based observations. The technique used most often in the past depended first on the identification of prominent lunar craters on earth-based photographs, and then a precise determination of their centers relative to a photographic coordinate system. Thus, the parallax in the positions of crater centers on photographs taken at different times could be observed and related to, among other things, the moon's figure. Reference 1 is an

example of a study utilizing this technique. The absolute accuracy of the resulting selenodetic system is limited, however, by the uncertainties in locating crater centers, in the dynamics of the earth-moon system, and in correcting for the atmospheric refraction of the earth.

The Lunar Orbiter series of spacecraft, for the first time, photographed approximately 99 percent of the surface of the moon with both high and moderate resolution cameras at altitudes ranging from 50 km (low lunar altitude) to approximately 2000 km. The resolving power of the moderate resolution camera at 50 km was 8 meters and that of the high resolution camera was 1 meter. Also, the individual photographs were taken in overlapping sequences. The overlap was as much as 86 percent. Also, in some instances, certain sites were rephotographed on successive orbits, successive missions, or both. These facts, coupled with the accuracy with which the spacecraft trajectory was determined, render these photographs useful in an analytical stereoscopic analysis of the Lunar Orbiter photographs for the purpose of determining the lunar size and shape, establishing a selenodetic datum, and aiding in the more accurate mapping of the moon.

This paper is an initial report on a continuing study of the moon's figure utilizing the Lunar Orbiter photographs. Since such a task requires years to complete, certain information is best presented as it is obtained. Thus, the concepts for performing the analytical stereoscopic analysis, the procedures established for reading the film, and some of the results obtained to date from mission I photography only are to be presented here.

The advantages of the Lunar Orbiter photographs over earth-based photography are obvious; the coordinates of very small craters may be observed on photographs taken outside the earth's atmosphere with a camera whose optical axis is nearly normal to the lunar surface.

For the purpose of analysis, a digital computer program was utilized to produce contour charts of sites by using lunar coordinates calculated from film readings of identifiable lunar features. These charts provide a convenient means for representing large quantities of data and may be utilized for terrain studies by other researchers. Since certain radii have been determined by other methods, such as the V/H sensor study and the Ranger impact data, the radii as read from the contour chart have been tabulated for purposes of comparison.

Other analyses are being performed at the Manned Spacecraft Center and at the Aeronautical Chart and Information Center and the Army Map Service of the Department of Defense with particular emphasis on lunar maps.

SYMBOLS

A	matrix of coefficients of equation of condition in **X**
a,b	photographic coordinates of an image
B	magnitude of base line
C	matrix of coefficients of equation of condition in **Y**
E	matrix of residuals
f	camera focal length
H	height of camera above feature
l	number of photographs in a sequence
n	number of features identified
P	lunar feature
p	image of feature
R	magnitude of radius vector to spacecraft
r	magnitude of selenocentric radius to feature
S,T,W	functions of camera attitude, focal length, and height
s	number of sequences
w	assigned weight
X,Y,Z	axes of rectangular Cartesian coordinate system
x,y,z	rectangular coordinates of a point
ϵ	residual

θ	swing component of camera attitude
ρ	line of projection of feature image through camera lens
σ	standard deviation
φ	roll component of camera attitude
τ	tilt component of camera attitude

Subscripts:

c	camera coordinate system
i	a particular lunar feature
j	a particular reference photograph or vector (j = 1, 2, . . .)
k	a particular reference photograph or vector (k = 1, 2, . . .)
n	intermediate reference photograph or vector
o	datum reference system, photograph, vector, or variable
p	photographic coordinate system
x,y,z	components of a variable
s,w	used to denote the particular function or condition for a residual

Notations:

$\{\ \}$	column matrix
$[\ ]$	square matrix
$\|\ \|$	rectangular matrix
*	least-squares estimate

Matrix exponents:

T	indicates the transpose
-1	indicates the inverse

A bar over a symbol indicates a vector. A bar below a symbol indicates an approximation. A prime indicates a transformed variable.

THEORY

The Lunar Orbiter mission 1 had a primary objective of providing overlapped sequences of photographs of selected primary (prospective Apollo landing sites) and secondary lunar sites with both high and moderate resolution cameras simultaneously and a secondary objective of providing precision trajectory information. The tracking data, however, were to support a study of the lunar gravitational field in addition to their fundamental function of permitting the spacecraft's orbit to be predicted. Thus, since the moderate resolution photographs overlapped by approximately 86 percent for most sequences (ref. 2), the photographs can be utilized, in conjunction with the orbital data, to accomplish the following objectives:

(1) Aid in a more accurate mapping of the lunar surface,

(2) Establish an approximation to the lunar geometric size and shape and the resulting selenodetic datum,

(3) Locate the lunar geometric center relative to the lunar center of mass, and

(4) Establish a mean spherical lunar radius in the equatorial region.

Definition of Coordinate Systems and Camera Attitude

Moon-stabilized coordinate system.- The fundamental system of reference in this study, shown in figure 1, is defined relative to the camera plane of motion as follows: The Z-axis is taken to be parallel to the radius vector from the center of gravity of the moon to the spacecraft at the time a particular photograph is exposed (termed the datum vector) and is positive outward. The Y-axis is taken to be in the plane of motion and perpendicular to the spacecraft radius vector and is positive in the direction of motion; and the X-axis is perpendicular to the plane of motion and completes the right-handed coordinate system. For convenience, the datum vector is chosen to be the state vector for that photograph nearest the center of the site being photographed.

Camera coordinate system.- The camera (X_c, Y_c, Z_c) coordinate system differs from the X,Y,Z system in that the Y_c axis is tilted τ degrees relative to Y and Z_c is rolled out of the plane of motion φ degrees (fig. 1) and is parallel to the camera optical axis. The X_c axis completes the right-handed system.

The roll and tilt angles define the attitude of the optical axis relative to the X,Y,Z system. However, the orientation of the film platten must be defined with the aid of a third coordinate system which is termed the photographic coordinate system.

Photographic coordinate system.- The photographic coordinate system is two-dimensional and lies in the plane of the photograph. Customarily, the photographic Y_p axis is chosen to be parallel to an edge of the camera platten and positive in the direction of motion, the X_p axis being normal to Y_p at the principal point (the intersection of the optical axis with the photographic plane) and positive to the right when viewed from above. Thus, since Y_p may or may not be parallel to plane of motion, the photograph is said to be swung θ degrees about the optical axis.

Significance of Coordinate Systems in Photographic Triangulation and Basic Approach to Problem

All image coordinates are observed relative to the photographic coordinate system and transformed into equivalent coordinates in the camera coordinate system. Thus, the Z_c coordinate of a feature is merely the projection of the distance from the image to the lens onto the optical axis.

Since the ratio of the camera focal length f to the spacecraft altitude above the lunar surface H is very small (approximately 1.7×10^{-5}), the negative plane is essentially at the camera focal plane. As a result, the Z_c coordinate of an image on the negative is equal to f.

In this paper, the photographic coordinates of an image are first transformed to the equivalent camera coordinates and then to the moon-stabilized system, which will be the fundamental system for photogrammetric reduction as stated above. Coordinates of a lunar feature are given in the selenographic system defined in the conventional manner.

The problem of deriving selenographic coordinates from the Lunar Orbiter photographs is discussed in the following steps:

(1) The basic expressions relating photographic coordinates to the moon-stabilized coordinates are derived for the case in which the attitude angles are each 0^o. Further, it is shown that these expressions must satisfy two conditions for each stereo pair and for each identifiable feature.

(2) The transformations necessary to obtain the equivalent normal photographic coordinates (0^o attitude) from photographic coordinates at any attitude are derived.

(3) It will be shown that the camera attitude can be determined from the photographic coordinates of the images and camera constants provided the spacecraft states corresponding to each photograph are known.

Spatial Triangulation of Lunar Orbiter Photography

Assumptions and equations of condition.- Prior to the photographing of a segment of the lunar surface, the spacecraft was oriented so that the optical axis would be, as nearly as possible, parallel to the local lunar radius at perilune and lie in the orbital plane or at a known angle to it. (See ref. 2.) Once the desired orientation was achieved, the spacecraft was gyro-stabilized and no new commands were given the spacecraft while the site was being photographed. Although there were drift rates associated with the gyros, the resulting change in attitude was insignificant. In view of these facts and the accuracy with which the spacecraft orbit was observed, it seems reasonable to assume the following:

(1) The spacecraft is translating in space with fixed orientation, although not precisely known, relative to the moon-stabilized system

(2) The spacecraft state vectors are known at the times of each photographic exposure.

With these assumptions in mind, consider figure 2 showing the spacecraft positions $\overline{R}_1$ and $\overline{R}_2$ which represent positions at which successive photographs are exposed. Note that $\overline{R}_1$ is shown as the datum vector and that, in accordance with these assumptions, the optical axes in figure 2 are represented as being parallel. In addition, the second photograph is represented as being displaced from the first along the X-axis since each state given in a fixed selenographic coordinate system is displaced slightly from the others along the X-axis because of the lunar rotation.

In figure 2, the camera attitude angles φ, θ, and τ are each 0^o. Then, according to convention, the photograph at $\overline{R}_1$ is said to be a "normal" photograph whereas the photograph at $\overline{R}_2$ is said to be "oblique" since the attitude angles for it are nonzero. Thus, if $\overline{R}_1$ is chosen to be the datum radius vector, the sequence of two photographs is termed "normal."

If the point P_i should be a feature on the lunar surface where the subscript i refers to the ith feature, the vectors $\rho_{i,1}$ and $\rho_{i,2}$ are projections of the images of P_i through the camera lens. The coordinates of the images of P_i on the two photographs are $a_{i,1},b_{i,1}$ and $a_{i,2},b_{i,2}$ and the vector joining the two spacecraft positions is termed the base vector $\overline{B}_{1,2}$. Then by vector addition,

$$\overline{B}_{1,2} = \overline{R}_2 - \overline{R}_1 \tag{1}$$

and

$$\overline{B}_{1,2} = \overline{\rho}_{i,1} - \overline{\rho}_{i,2} \tag{2}$$

whereas

$$\overline{r}_i = \overline{R}_1 + \overline{\rho}_{i,1} = \overline{R}_2 + \overline{\rho}_{i,2} \tag{3}$$

is the selenocentric radius vector from the lunar center of mass to the feature P_i.

For convenience, it is assumed that the spacecraft states are known in the system when the origin is at the lunar center of mass. Since $\overline{R}_1$ in figure 2 is defined as the datum vector, the altitude of the spacecraft above the point P_i at the first position is $H_{o,i}$ (the subscript o implies that the height is measured parallel to the datum vector) with

$$\rho_{z,i,2} = H_{2,i} = H_{o,i} + \Delta H = H_o + B_{z,1,2} = \rho_{z,i,1} + B_{z,1,2} \tag{4}$$

at the second position. If equation (1) should be resolved into its components,

$$\left.\begin{aligned} B_{x,1,2} &= R_{x,2} - R_{x,1} \\ B_{y,1,2} &= R_{y,2} - R_{y,1} \\ B_{z,1,2} &= R_{z,2} - R_{z,1} \end{aligned}\right\} \tag{5}$$

and if equation (2) is resolved into its components,

$$\left.\begin{aligned} B_{x,1,2} &= \rho_{x,i,1} - \rho_{x,i,2} \\ B_{y,1,2} &= \rho_{y,i,1} - \rho_{y,i,2} \\ B_{z,1,2} &= \rho_{z,i,1} - \rho_{z,i,2} \end{aligned}\right\} \tag{6}$$

As will be shown later, the expression for the Z component of $\overline{\rho}_1$ is a function of $B_{z,1,2}$, the camera attitude and focal length, and the photographic coordinates of the image of P_i on both photographs. Thus, the expression for $\rho_{z,i,2}$ is identical to that for $\rho_{z,i,1}$ plus the Z component of $\overline{B}$ which is assumed to be known from equation (5). As a result, the first two expressions are the condition equations which must be satisfied by the photography.

Moon-stabilized coordinates of a feature.- To find expressions for the components of the $\overline{\rho}_{i,j}$ vectors, consider, again, figure 2. The x and y components of the vectors $\overline{\rho}_{i,1}$ and $\overline{\rho}_{i,2}$ are by similar triangles

$$\left.\begin{aligned}
\rho_{x,i,1} &= x_{i,1} = -H_{o,i}\frac{a_{i,1}}{f} \\
\rho_{y,i,1} &= y_{i,1} = -H_{o,i}\frac{b_{i,1}}{f} \\
\rho_{x,i,2} &= x_{i,2} = -\left(H_{o,i} + B_{z,1,2}\right)\frac{a_{i,2}}{f} \\
\rho_{y,i,2} &= y_{i,2} = -\left(H_{o,i} + B_{z,1,2}\right)\frac{b_{i,2}}{f}
\end{aligned}\right\} \qquad (7)$$

The attitude of the spacecraft camera as portrayed in figure 2 is that of a "normal" photograph at position 1 where, in general, the Lunar Orbiter photography must be considered oblique. For oblique photography (photographs taken with a camera whose attitude is not normal), it can be shown that the components of $\rho_{1,i}$ and $\rho_{2,i}$ are given by expressions similar to those in equation (7). In figure 2, the photographic coordinates of the images of p_i are given by $a_{i,1},b_{i,1}$ and $a_{i,2},b_{i,2}$ in the first and second photographs, respectively. Further, since the photographs are represented as being of normal attitude, the equivalent x,y,z coordinates of the image in the first photograph in the X,Y,Z system were merely $a_{i,1},b_{i,1},f$ with similar coordinates for the second photograph. If, however, the photographs were oblique views of the moon, the photographic coordinates of the images of P_i would have to be transformed into the equivalent coordinates in the X,Y,Z systems. Thus, if $a'_{i,j}$, $b'_{i,j}$, and $f'_{i,j}$ should represent these transformed coordinates, they would be those photographic coordinates which would have been observed if the photograph had been normal. As a result, the expressions of equation (7) can be rewritten in a more general form as

$$\left.\begin{aligned}
-\left(H_{o,i} + B_{z,o,j}\right)\frac{b'_{i,j}}{f'_{i,j}} &= y_{i,j} = \rho_{y,i,j} \\
-\left(H_{o,i} + B_{z,o,j}\right)\frac{a'_{i,j}}{f'_{i,j}} &= x_{i,j} = \rho_{x,i,j} \\
-\left(H_{o,i} + B_{z,o,k}\right)\frac{b'_{i,k}}{f'_{i,k}} &= y_{i,k} = \rho_{y,i,k} \\
-\left(H_{o,i} + B_{z,o,k}\right)\frac{b'_{i,k}}{f'_{i,k}} &= x_{i,k} = \rho_{x,i,k}
\end{aligned}\right\} \qquad (8)$$

where the prime indicates that the photographic coordinates have been transformed, $B_{Z,o,j}$ and $B_{Z,o,k}$ represent the Z components of the base line relative to the datum vector in the X,Y,Z system. The subscripts i, j, and k refer to the identification number of the feature in the first and second photographs, respectively, of the combination being considered.

Transformation equations.- To obtain the equations of transformation, consider figure 3 in which the camera has a swing angle of θ degrees in the plane of the oblique photograph, a tilt angle of τ degrees in the Y_C,Z_C plane, and a roll angle of φ degrees in the Z_O,X_O plane where the subscript o indicates the X,Y,Z system. Inasmuch as the photograph is depicted in the figure as a positive photograph, the calibrated camera focal length f is denoted as being negative since the positive plane must be, by definition, on the object side of the camera lens. For a negative photographic plane (one), the focal length f would be positive, and the image coordinates would be the negative of those observed in the positive plane. The coordinates $a_{i,j},b_{i,j}$ in the photographic system transform into those in the X,Y,Z system by the expressions

$$\left.\begin{aligned} a'_{i,j} &= \left(a_{i,j}\cos\theta + b_{i,j}\sin\theta\right)\cos\varphi - f\sin\varphi \\ b'_{i,j} &= \left\{\left(b_{i,j}\cos\theta - a_{i,j}\sin\theta\right)\cos\tau + \left[f\cos\varphi + \left(a_{i,j}\cos\theta + b_{i,j}\sin\theta\right)\sin\varphi\right]\sin\tau\right\} \\ f'_{i,j} &= \left\{\left[f\cos\varphi + \left(a_{i,j}\cos\theta + b_{i,j}\sin\theta\right)\sin\varphi\right]\cos\tau - \left(b_{i,j}\cos\theta - a_{i,j}\sin\theta\right)\sin\tau\right\} \end{aligned}\right\} \quad (9)$$

when the order of transformation is first through the angle θ, then the angle φ, and finally the angle τ. Thus, the expressions for $\rho_{x,i,j}$ and $\rho_{y,i,j}$ are

$$\left.\begin{aligned} \rho_{x,i,j} &= F_x\left(f,a_{i,j},b_{i,j},\theta,\varphi,\tau,H_{o,i},B_{Z,o,j}\right) = x_{i,j} \\ \rho_{y,i,j} &= F_y\left(f,a_{i,j},b_{i,j},\theta,\varphi,\tau,H_{o,i},B_{Z,o,j}\right) = y_{i,j} \end{aligned}\right\} \quad (10)$$

in which every variable is known except $H_{o,i}$.

By equations (1) and (5)

$$B_{y,j,k} = R_{y,k} - R_{y,j} = \rho_{y,k,j} - \rho_{y,i,k} \quad (11)$$

Substituting the appropriate relations from equations (8) and solving equation (11) yields

$$H_{o,i} = - \frac{B_{y,j,k} + B_{z,o,j} \frac{b'_{i,j}}{f'_{i,j}} - B_{z,o,k} \frac{b'_{i,k}}{f'_{i,k}}}{\frac{b'_{i,j}}{f'_{i,j}} - \frac{b'_{i,k}}{f'_{i,k}}} \tag{12}$$

It is now possible to solve for the selenographic coordinates of a lunar feature P_i with the aid of the relations in equations (3), (8), (9), (10), and (12), provided the camera attitude is known and the photographic coordinates of the images of P_i can be obtained.

Least-squares estimate to the camera attitude.- The camera attitude can be found by perturbing the attitude about the nominal in such a way as to find that attitude which will minimize the sum of the squares of the distances between all combinations of $\overline{\rho}_{i,j}$ vectors to the feature P_i for all the lunar features simultaneously.

Before continuing, however, it is desirable to rewrite the first two relations of equations (5) and (12) in their more general form. First, let

$$H_{o,i} = T_{i,j,n}\left(f, a_{i,j}, a_{i,n}, b_{i,j}, b_{i,n}, \theta, \varphi, \tau, B_{z,b,j}, B_{z,o,n}, B_{y,j,n}\right) \tag{13}$$

and

$$\left.\begin{aligned} B_{x,j,k} &= \rho_{x,i,j} - \rho_{x,i,k} = W_{i,j,k}\left(f, a_{i,j}, a_{i,k}, b_{i,j}, b_{i,k}, \theta, \varphi, \tau, T_{i,j,n}, B_{z,o,j}, B_{z,o,k}\right) \\ B_{y,j,k} &= \rho_{y,k,j} - \rho_{y,i,k} = S_{i,j,k}\left(f, a_{i,j}, a_{i,k}, b_{i,j}, b_{i,k}, \theta, \varphi, \tau, T_{i,j,n}, B_{z,o,j}, B_{z,o,k}\right) \end{aligned}\right\} \tag{14}$$

where S, W, and T are functions of several variables and n is a constant subscript equal to j,k or some other photographic index to which p_i is common. The subscript n implies that the partial derivatives of $T_{i,j,n}$ are to be evaluated using nth photograph in conjunction with the jth photograph. The subscript n is then incremented until all possible values are used. However, n changes only when j changes.

Since S, T, and W are nonlinear in θ, τ, and φ,

$$\left.\begin{aligned} B_{x,j,k} = \underline{W}_{i,j,k} &+ \left(\frac{\partial W_{i,j,k}}{\partial \theta} + \frac{\partial W_{i,j,k}}{\partial H_{o,i}} \frac{\partial T_{i,j,n}}{\partial \theta}\right) d\theta + \left(\frac{\partial W_{i,j,k}}{\partial \tau} + \frac{\partial W_{i,j,k}}{\partial H_{o,i}} \frac{\partial T_{i,j,1}}{\partial \tau}\right) d\tau \\ &+ \left(\frac{\partial W_{i,j,k}}{\partial \varphi} + \frac{\partial W_{i,j,k}}{\partial H_{o,i}} \frac{\partial T_{i,j,1}}{\partial \varphi}\right) d\varphi \end{aligned}\right\}$$

(Equations continued on next page)

$$B_{y,j,k} = \underline{S}_{i,j,k} + \left(\frac{\partial S_{i,j,k}}{\partial \theta} + \frac{\partial S_{i,j,k}}{\partial H_{o,i}} \frac{\partial T_{i,j,n}}{\partial \theta}\right) d\theta + \left(\frac{\partial S_{i,j,k}}{\partial \tau} + \frac{\partial S_{i,j,k}}{\partial H_{o,i}} \frac{\partial T_{i,j,n}}{\partial \tau}\right) d\tau + \left(\frac{\partial S_{i,j,k}}{\partial \varphi} + \frac{\partial S_{i,j,k}}{\partial H_{o,i}} \frac{\partial T_{i,j,n}}{\partial \varphi}\right) d\varphi \qquad (15)$$

are the first-order Taylor expansions of equations (14), where the bars under S and W indicate that they are approximate values of the expressions as calculated from the observed coordinates of the images of P_i and the nominal camera attitude and height. Thus, from equations (6), (14), and (15), the two equations of condition became

$$\left.\begin{aligned} \epsilon_{w,i,j,k} &= B_{x,j,k} - \underline{W}_{i,j,k} \\ \epsilon_{s,i,j,k} &= B_{y,j,k} - \underline{S}_{i,j,k} \end{aligned}\right\} \qquad (16)$$

where the ϵ terms are the residuals.

Each relation in equations (16) is an independent relation which must be satisfied. Thus,

$$\sum_{i}^{n} \sum_{j}^{l} \sum_{k}^{l} \left(\epsilon_{w,i,j,k}^2 + \epsilon_{s,i,j,k}^2\right) = \text{Minimum}$$

is the least-squares condition to which a solution is sought.

Thus, if A is an $nl^2 \times 3$ weighted matrix of the partial derivatives in the first expression in equations (16) and C is the similar matrix of partials in the second expression, then, if E_W is the nl^2 weighted column matrix of residuals ϵ_W in equations (16) and E_S the equivalent matrix for ϵ_S,

$$\begin{Bmatrix} \Delta\theta \\ \Delta\tau \\ \Delta\varphi \end{Bmatrix}^* = \left[\left[\|A\|^T \|A\|\right] + \left[\|C\|^T \|C\|\right]\right]^{-1} \left[\|A\|^T \{E_W\} + \|C\|^T \{E_S\}\right] \qquad (17)$$

where the * beside the column matrix indicates a least-squares estimate to the errors in the assumed values of roll, swing, and tilt. (See the appendix for the appropriate partial derivatives in eqs. (15).)

Computational Technique

In the preceding discussion it has been shown that the selenocentric radii to selected lunar features can be computed from photographic coordinates by first finding that most probable attitude of the spacecraft camera which will minimize the sums of the squares between all combinations of ρ vectors. Because the expressions derived are nonlinear in θ, τ, and φ, the method of solution is an iterative technique. The order of solution is as follows:

(1) Assume a nominal attitude

(2) Compute components of states in X,Y,Z systems

(3) Screen for inconsistent and duplicated data and correct for lens distortion

(4) Compute coefficients and the corresponding residuals necessary for solution of equation (18) for all combinations of photographs and all features

(5) Find the best estimate to the camera attitude and iterate, if time corrections are not desired, until the attitude has converged satisfactorily

(6) If time corrections are desired, compute correction to states as a function of time necessary to minimize the sum of the squares of the differences between the mean selenocentric coordinates of each feature and the coordinates obtained from each photograph to which the feature is common for all the features

(7) Repeat preceding steps if necessary

(8) Compute the mean selenocentric coordinates of each feature using the observed coordinates and estimated attitude for each photograph.

Each expression in equations (16) was weighted by the expression

$$w^2_{i,j,k} = \left(\frac{f^2}{f^2 + a^2_{i,j} + b^2_{i,j}} + \frac{f^2}{f^2 + a^2_{i,k} + b^2_{i,k}} \right) \frac{\left|\overline{B}_{j,k}\right|}{H_{o,i}} \tag{18}$$

which was determined empirically.

Before continuing it is necessary to point out that a given feature will not necessarily be on the datum photograph. Thus, in practice an intermediate photograph called a reference photograph was chosen and the resulting error equations for each possible combination were computed. The process was then repeated with a new reference until all possible combinations were used. In each case the coefficients for equations (15) were recomputed only when a new reference was chosen.

LUNAR ORBITER PHOTOGRAPHIC DATA CHARACTERISTICS AND READING PROCEDURES

Characteristics of Lunar Orbiter Photographs

The Lunar Orbiter spacecraft film was automatically processed and dried onboard the spacecraft as it was exposed. The photographic data on the exposed film was then converted by the readout system into electrical form and transmitted to ground-based receiving stations where it was recorded on tape. This conversion was accomplished, in part, by first scanning the film with a high-intensity beam of light 2.677 mm parallel with the film edge and, then, advancing the scan line along the width of the film until the opposite edge was reached. Upon reaching the opposite edge of the 70-mm film, the film was advanced 2.54 mm and the process of scanning was repeated. With each advance of the film, the scan line advance proceeded in a direction across the film opposite to the previous one. All the photographic data transmitted while scanning across the film in one direction comprised one framelet. Each framelet of photographic data was reproduced, with the aid of a kinescope tube, on 35-mm film which was, in turn, used to reconstruct the Lunar Orbiter photographs. (A moderate resolution photograph is composed of approximately 26 framelets and is termed a composite here.)

The photograph shown in figure 4 is typical of the Lunar Orbiter photographs used in this study, and in figure 5 part of one framelet is shown.

Along the upper edge of the photograph in figure 4, it will be noted that there is a repeating pattern of gray scales, vertical, horizontal, and diagonal lines, and so forth, with an identifying three-digit number preceding each gray scale and a continuous series of small rectangles called edge data. (Also, see fig. 5.) Further, a series of notches called sawteeth appear on both the upper and lower edges of the format of the photograph.

The edge data were preprinted on the spacecraft 70-mm film with the aid of a master copy of edge data containing gray scales numbered from 000 to 999. This master copy was carefully designed and made to strict specifications. Thus, the edge data are independent of camera distortion.

The sawteeth were machined in the platten of each camera, and as a result are a physical part of the camera. Thus, the X_p and Y_p coordinates of each sawtooth were determined as a part of the calibration data relative to the principal point. Each sawtooth was assigned a number. (There are 84 sawteeth for the moderate resolution camera, the 43d and 44th sawteeth being nearest the camera principal point.) In the calibration report the even numbers refer to the sawteeth adjacent to the film edge data and the odd numbers refer to the sawteeth on the opposite edge.

Film Reading Procedures

The composite in figure 4 is used in this study for feature selection and identification and as a permanent record of the selected features. The X and Y coordinates of the feature, once identified, are measured on the 35-mm framelet with a comparator.

A comparator is a precision x,y measuring instrument utilizing two screws oriented in such a way as to permit a carriage to be driven in a plane along two perpendicular directions which simulate the X- and Y-axes of a rectangular Cartesian coordinate system. The mutually perpendicular Z-axis is defined as being parallel to the optical axis of a viewing telescope which remains fixed. A table mounted on the carriage and parallel to the X,Y plane can be rotated about the Z-axis to permit alinement with the X- or Y-axis. Thus, the X,Y coordinates of one point relative to another can be measured on the comparator as a function of the number of turns of the screws; these turns are convertible into units of measure.

For the case of nonskewed framelets (rectangular), the ideal comparator alinement is such that the comparator X-axis be parallel to the framelet photographic data edge (the long edge of the image of the framelet, fig. 5). Thus, since no skewness was observed for mission I photography, before initiating measurements on a framelet the comparator alinement was adjusted so that this condition would be fulfilled. As for a point of origin for X and Y measurements, the upper left-hand corner of the gray scale (the location of the white cross in fig. 5) was chosen as the comparator reference point.

In figure 5 the distance between the gray-scale reference point (represented by the cross) and the corresponding point on the neighboring gray scale (represented by the dot inside the square) is defined as the gray-scale separation. (The gray-scale separation could not be observed on all framelets.) The ratio of the gray-scale separation as observed on the comparator to the corresponding distance on the spacecraft film is the magnification factor. Division of the comparator coordinates by the magnification factor converts them to the spacecraft equivalent. The gray-scale separation together with the identifying number for each comparator gray-scale reference provides a convenient means for transferring observations from one framelet to another. Thus, to obtain the best possible value for the gray-scale separation, its measured magnitude was averaged over the whole mission.

To obtain photographic coordinates of a feature, it was necessary to measure the comparator coordinates of either the 43d or 44th sawtooth which are nearest the principal point. For this purpose, the 44th sawtooth was chosen since it is nearest the edge data. Since the X coordinate of the 44th sawtooth should remain constant over the whole mission, its average comparator value over the mission was assumed to be correct as was the case with the gray-scale separation measurement.

Feature Selection and Size

Features were chosen on the composite sufficiently small to be considered points and yet sharp enough to be quickly distinguished. A feature fitting this description will, on the composite, appear to be about the size of a reasonably sharp pencil point. According to comparator measurements, such a feature will, at lunar scale, rarely exceed 25 meters in diameter. It is estimated that it can be positioned relative to the crosshairs in the comparator to an accuracy of about 4 meters at the lunar scale.

As to the distribution of selected features, an attempt was made to select features so that there would be a larger concentration of points near an imaginary line extending linearly down that framelet containing the 44th sawtooth. This procedure will have a tendency to give greater weight (in the attitude evaluation) to data near the optical axes where the optical distortion is the least.

In order to demonstrate the desired distribution of features on the composite, figure 6 depicts those features selected on the photograph in figure 4 as white dots. The size of the dot is in no way related to feature size or uncertainty but is purely for the purpose of viewing ease.

Once the features on a photograph were selected, each was given an identifying number and then transferred to all other photographs of the site. With each additional photograph, features were added at the rate of about 15 per photograph. The first and last photographs in the sequence had no additional features identified thereon.

RESULTS AND DISCUSSION

To date, all the photographs from seven mission I sequences have been read. In order to give an idea as to the approximate position of each sequence in latitude and longitude, each has been presented in table I and in figure 7. Beside each sequence in table I is the maximum number of points identified on each site along with other pertinent data which are discussed later. The mission number is denoted by I, the primary site is designated by P; Arabic numeral denotes order in which site was photographed, and the letters A and B denote consecutive orbits.

As will be noted, all the primary sequences in mission I are included in table I with the exceptions of I P-3, I P-4, and I P-6. Site I P-3 is currently being read and no plans exist for observing the remaining sites since the included photography overlaps by approximately 50 percent.

Accuracy of Analysis

Before discussing the results, it is of interest to outline various uncertainties which can be expected in the results of this report. As stated earlier, the method of

computation consists of determining the best estimate to the camera attitude relative to a datum state. The resulting estimated camera attitudes are given in table I, for all the sequences processed, along with the datum state for each sequence. It will be noted that site I P-9.2 is the only site for which the roll component of attitude was determined. This condition results from the fact that roll angle cannot be established except in those cases where there is side-lapping photography. There will result one set of three attitude angles for each sequence of side-lapping photography. See appendix for details.

Any errors which may be considered as being random, such as the relative errors in photographic times, comparator errors, and so forth will be reflected in the standard deviations of each radius (or attitude). On the other hand, however, bias errors such as the absolute photographic time associated with the datum state and its uncertainty in position will be reflected as a bias in the latitude and longitude of each feature and can only be estimated.

In an effort to reduce the relative errors in time, 0.05 second was added to each spacecraft time since it was truncated to the nearest 0.1 sec. This procedure results in a maximum relative error in base of ±141 meters and reflects directly into a radius determination. Since the simultaneous solution of sequences of photography obtained from consecutive orbits should yield the largest internal errors due to orbital uncertainties, site I P-9.2 was assumed to be representative of all sequences as reported herein.

As stated, the computational procedure is an iterative one. Thus, to check the convergence of the individual components of attitude, the data for the two sequences of photographic data from site I P-9.2 were processed by using 20 iterations, the initial camera attitude being normal, and the individual estimated attitude corrections were printed after each.

In figure 8, the resulting corrections are plotted for both sequences as a function of the number of iterations. From the curves it is seen that the components of attitude converge although the first estimate was too large (represented by the dashed line). After 12 iterations, the corrections have, for all practical purposes, reached zero radians; thus, 20 iterations are deemed to be more than adequate to achieve the desired attitudes.

Since some features were found to appear on as many as 10 photographs in a given sequence (as many as 20 photographs in the case of site I P-9.2), the selenographic coordinates of each feature were computed for every photograph on which it appeared, and the resulting coordinates were averaged. In figure 9, the frequency distribution of the standard deviations of the mean of the resulting radii for all the features identified on sites I P-9.2A and I P-9.2B are plotted. From the plot, it is seen that better than 30 percent have standard deviations of the mean of 25 meters or less. Most of the features have coordinates with standard deviations of less than ±45 meters.

As expected, it was found that the standard deviations were greatest for those features common to only two photographs and dropped off rapidly with an increase in number. A standard deviation of the mean of ±200 meters was found to encompass all those radii which could be considered under any condition to be good. Only 10 percent of the points in sites I P-9.2A and I P-9.2B were found to have standard deviations greater than 85 meters.

Thus, from the foregoing statement, it can be concluded that in the worst cases a maximum standard deviation of 200 meters can be expected and 20 iterations are more than adequate to establish the camera attitude. Therefore, the internal consistency of the resulting lunar coordinates is excellent.

As for bias errors, it has been determined that the spacecraft state is known to an accuracy of 3 km. This accuracy will result in an uncertainty of 2.7-km circular error at the lunar surface. Bias errors have been found to be relatively insignificant in the spacecraft radius. (See ref. 3.)

Contour Charts

To facilitate the presentation of lunar coordinates and radii, the digital computer program for generating contour charts reported in reference 4 was modified and adapted to this computing facility, and contour charts for sites listed in table I were generated since such a representation is better for presenting large masses of data. The resulting charts are shown in figures 10 to 15, respectively.

The contouring interval was taken to be 100 meters and represents elevations above a sphere of 1735.000 km. The grid was obtained by projecting the spherical coordinates onto a cylinder which had its transverse axis parallel to the lunar spin axis and was tangent to the sphere at 0^{o} latitude.

The digital program, in brief, generates a matrix of terrain elevations (termed a depth matrix) from the latitudes and longitudes associated with the elevations given it, and interpolates and extrapolates to fill out the matrix. In so doing, it is assumed that each row in the matrix represents a line of latitude and each column represents a line of longitude. Thus, a rectangular strip of the lunar surface which is inclined slightly to the lines of latitude such as a Lunar Orbiter site will be represented by a slightly larger rectangle with 0^{o} inclination and this fact should be kept in mind when the results are compared.

The charts show rises and depressions as is expected. However, there are no real radical slope changes except in the case of I P-1 and I P-2 shown in figures 10 and 11. At approximately 34^{o} longitude in figure 11, there are two rather sharp depressions which are borne out by the radical change in shadows on the photographs themselves. The same

can be said for the other sequences. However, because of the overexposure of some frames during reproduction, they are not as conclusive.

None of the charts show an elevation difference greater than 2.8 km. Most of the radii appear to lie within the region of about 1736.0 ± 1.5 km. In fact, the arithmetic mean of all radii was found to be 1735.697 km.

In the case of I P-9.2 in figure 15, most of the elevations lie within the region of 300 ± 100 m. There is, however, a small depression beginning at approximately 44° west longitude and 3.4° south longitude and continuing west of south. Such a depression has been reported to exist in an oblique view of this site taken from a later mission.

Sites I P-1 and I P-2 seem to be slightly more rugged than the remaining sites in that there is a greater variation in elevation of the site. In the main, however, all do appear, with the exception of I P-7, to have elevations ranging from 300 to 1300 meters (if the radical terrain changes are ignored) or an average of about 800 ± 500 meters. Sites I P-5 and I P-7 are higher than any of the other sites with an average elevation of 1100 ± 500 meters. In no case is the elevation seen to rise above 1737.5 km.

Careful examination of the charts will show a slight increase in radius as the lunar prime meridian is approached; this increase implies an equatorial ellipticity. As a result, all coordinates were processed together in an attempt to fit by the method of least squares an ellipse to the data. The resulting semiaxes were 1736.589 km and 1734.213 km in the prime meridian and at the limbs, respectively. No weighting was utilized to minimize the effects of mountains and valleys on the resulting ellipse. Thus, the results are slightly in error.

Thus, based on these observations, it seems reasonable to say that the mean lunar radius is approximately 2 km shorter than the assumed value of 1738 km, and that there is an apparent slight bulge in the region of Sinus Medii. However, before any definite statements regarding the lunar bulge can be made, more sites will have to be processed and the data treated analytically as a whole.

Comparison of Results With Those of Other Studies

In reference 5 the velocity to height ratios V/H read from a spacecraft camera motion compensation device as part of the spacecraft telemetry have been converted to lunar radii. In table II, several of the resulting radii are tabulated along with the corresponding radius as read from the contour charts contained herein. Each point in table II has been given a number and is represented on the appropriate contour chart with a black dot. As can be seen from table II, the maximum difference is 1.02 km whereas the minimum difference is 0.02 km. The best overall comparison was obtained on site I P-9.2, which is a simultaneous solution of two sequences of photography. Thus, it can be stated that the two independent approaches are in good agreement with each other.

Like the Lunar Orbiter spacecraft, the Ranger series of spacecraft were designed to photograph the lunar surface. However, unlike the Lunar Orbiter, Ranger was flown on an impact trajectory and televised each photograph as it was taken. Since the scan rates of the television camera and so forth were known, it was possible to count the number of scan lines of the last photograph to be televised for each mission and, as a result, compute very accurately the impact times which in conjunction with the tracking data could then be converted into lunar radii of a high quality. (See ref. 6.)

In table III the results of this experiment as reported in reference 6 are tabulated for comparison here. As will be noted, none of the radii lie on any of the charts contained herein. Thus, no direct comparison can be made. However, from a qualitative point of view, there is no denying that the radii deduced from the photography are in good agreement with those of the Ranger, especially since the arithmetic mean of the Ranger obtained radii is 1735.425 km which agrees favorably with the value of 1735.697 km determined herein.

CONCLUDING REMARKS

It has been shown that the lunar radii can be derived from the Lunar Orbiter photography by photogrammetric techniques with an excellent internal consistency and a standard deviation of the mean not exceeding 200 meters. The consistency of results between sequences was of such quality that a sphere of 1736.0 ± 1.5 km encompassed essentially all radii including mountain peaks and valleys. As a result, it is concluded that the mean lunar radius is closer to 1736.0 km than the currently accepted value of 1738 km.

Upon comparing the radii determined photogrammetrically with 14 isolated points determined from V/H data, an average difference of 486 meters was found to exist. A difference of only 457 meters was found to exist between the V/H points nearest the centers of the contour charts (absolute values were used for averaging). The average radius of 1735.425 km determined from the four Ranger points is in good agreement with that of 1735.697 km determined photogrammetrically. Thus, the three independent techniques are consistent with each other and add emphasis to the statement that the currently accepted value of the mean lunar radius is in error. It should be pointed out, however, that the radii contained herein are from the lunar center of gravity which is not necessarily the lunar geometric center.

Langley Research Center,
National Aeronautics and Space Administration,
Langley Station, Hampton, Va., March 28, 1969,
185-42-12-01-23.

APPENDIX

COEFFICIENTS FOR CONDITION EQUATIONS

The expressions in equations (8), (9), (12), and (15) are general for a single sequence of photography only. If a solution should be attempted for two or more side-lapping sequences of photography, the attitude angles φ, θ, and τ require subscripts since they are constant over a single sequence of photography only. In such an event the expressions in equations (15) would contain coefficients for each additional set of attitude angles since W, S, and T would then contain $3(s - 1)$ additional variables where S implies the number of sequences.

The partials of W and S in equations (15) are as follows:

$$\frac{\partial W_{i,j,k}}{\partial \theta} = \frac{\partial \rho_{x,i,j}}{\partial \theta} - \frac{\partial \rho_{x,i,k}}{\partial \theta}$$

$$\frac{\partial W_{i,j,k}}{\partial \tau} = \frac{\partial \rho_{x,i,j}}{\partial \tau} - \frac{\partial \rho_{x,i,k}}{\partial \tau}$$

$$\frac{\partial W_{i,j,k}}{\partial \varphi} = \frac{\partial \rho_{x,i,j}}{\partial \varphi} - \frac{\partial \rho_{x,i,k}}{\partial \varphi}$$

$$\frac{\partial W_{i,j,k}}{\partial H_{O,i}} = \frac{\partial \rho_{x,i,j}}{\partial H_{O,i}} - \frac{\partial \rho_{x,i,k}}{\partial H_{O,i}}$$

$$\frac{\partial S_{i,j,k}}{\partial \theta} = \frac{\partial \rho_{y,i,j}}{\partial \theta} - \frac{\partial \rho_{y,i,k}}{\partial \theta}$$

$$\frac{\partial S_{i,j,k}}{\partial \tau} = \frac{\partial \rho_{y,i,j}}{\partial \tau} - \frac{\partial \rho_{y,i,k}}{\partial \tau}$$

$$\frac{\partial S_{i,j,k}}{\partial \varphi} = \frac{\partial \rho_{y,i,j}}{\partial \varphi} - \frac{\partial \rho_{y,i,k}}{\partial \varphi}$$

$$\frac{\partial S_{i,j,k}}{\partial H_{O,i}} = \frac{\partial \rho_{y,i,j}}{\partial H_{O,i}} - \frac{\partial \rho_{y,i,k}}{\partial H_{O,i}}$$

where the partials of $\rho_{x,i,j}$ and $\rho_{y,i,j}$ are found from the appropriate expressions in equations (8) to be

$$\frac{\partial \rho_{x,i,j}}{\partial \theta} = - \frac{(H_{o,i} + B_{z,o,j})}{(f'_{i,j})^2} \left(f'_{i,j} \frac{\partial a'_{i,j}}{\partial \theta} - a'_{i,j} \frac{\partial f'_{i,j}}{\partial \theta} \right) - \frac{x_{i,j}}{H_{o,i} + B_{z,o,j}} \frac{\partial H_{o,i}}{\partial \theta}$$

$$\frac{\partial \rho_{x,i,j}}{\partial \tau} = - \frac{(H_{o,i} + B_{z,o,j})}{(f'_{i,j})^2} \left(f'_{i,j} \frac{\partial a'_{i,j}}{\partial \tau} - a'_{i,j} \frac{\partial f'_{i,j}}{\partial \tau} \right) - \frac{x_{i,j}}{H_{o,i} + B_{z,o,j}} \frac{\partial H_{o,i}}{\partial \tau}$$

$$\frac{\partial \rho_{x,i,j}}{\partial \varphi} = - \frac{(H_{o,i} + B_{z,o,j})}{(f'_{i,j})^2} \left(f'_{i,j} \frac{\partial a'_{i,j}}{\partial \varphi} - a'_{i,j} \frac{\partial f'_{i,j}}{\partial \varphi} \right) - \frac{x_{i,j}}{H_{o,i} + B_{z,o,j}} \frac{\partial H_{o,i}}{\partial \varphi}$$

$$\frac{\partial \rho_{y,i,j}}{\partial \theta} = - \frac{(H_{o,i} + B_{z,o,j})}{(f'_{i,j})^2} \left(f'_{i,j} \frac{\partial b'_{i,j}}{\partial \theta} - b'_{i,j} \frac{\partial f'_{i,j}}{\partial \theta} \right) - \frac{y_{i,j}}{H_{o,i} + B_{z,o,j}} \frac{\partial H_{o,i}}{\partial \theta}$$

$$\frac{\partial \rho_{y,i,j}}{\partial \tau} = - \frac{(H_{o,i} + B_{z,o,j})}{(f'_{i,j})^2} \left(f'_{i,j} \frac{\partial b'_{i,j}}{\partial \tau} - b'_{i,j} \frac{\partial f'_{i,j}}{\partial \tau} \right) - \frac{y_{i,j}}{H_{o,i} + B_{z,o,j}} \frac{\partial H_{o,i}}{\partial \tau}$$

$$\frac{\partial \rho_{y,i,j}}{\partial \varphi} = - \frac{(H_{o,i} + B_{z,o,j})}{(f'_{i,j})^2} \left(f'_{i,j} \frac{\partial b'_{i,j}}{\partial \varphi} - b'_{i,j} \frac{\partial f'_{i,j}}{\partial \varphi} \right) - \frac{y_{i,j}}{H_{o,i} + B_{z,o,j}} \frac{\partial H_{o,i}}{\partial \varphi}$$

The expressions for the partials of $\rho_{x,i,k}$ and $\rho_{y,i,k}$ are identical to the preceding equations with the exception of a change of the j subscript to k. The same is true for the partials of $a'_{i,j}$ and $a'_{i,k}$, and so forth. Therefore they are not written here.

Although the expression for $H_{o,i}$ as given by equation (12) is wholly adequate and is entirely correct, from the standpoint of programing ease, a more adaptable expression is desirable.

Consider the case for normal photography where the z-components of the base vector are zero. Then equation (12) becomes

$$H_{o,i} = - \frac{B_{y,j,k,f}}{b_{i,j} - b_{i,k}}$$

but, from equation (7),

$$b_{i,j} = y_{i,j} \frac{f}{H_{o,i}}$$

and

$$b_{i,k} = y_{i,k} \frac{f}{H_{o,i} + B_{z,o,j}}$$

whereby $H_{o,i}$ is a function of itself

$$H_{o,i} = - \frac{B_{y,j,k}(H_{o,i} + B_z)}{y_{i,j} - y_{i,k}}$$

Thus, after expanding into a Taylor series and neglecting all terms higher than first degree,

$$H_{o,i} - \underline{H}_{o,i} = \Delta H_{o,i} = - \frac{B_{y,j,k}}{y_{i,j} - y_{i,k}} dH_{o,i} + \frac{B_{y,j,k}(H_{o,i} + B_{z,o,j})}{(y_{i,j} - y_{i,k})^2} \left[\frac{\partial(y_{i,j} - y_{i,k})}{\partial \theta} d\theta \right.$$

$$\left. + \frac{\partial(y_{i,j} - y_{i,k})}{\partial \varphi} d\varphi + \frac{\partial(y_{i,j} - y_{i,k})}{\partial \tau} d\tau + \frac{\partial(y_{i,j} - y_{i,k})}{\partial H_{o,i}} dH_{o,i} \right]$$

and, if $\Delta H_{o,i}$ is allowed to become sufficiently small,

$$dH_{o,i} = \left\{ \frac{B_{y,j,k}(H_{o,i} + B_{z,o,j})}{\left[(y_{i,j} - y_{i,k})^2 + B_{y,j,k}(y_{i,j} - y_{i,k}) \right] - B_{y,j,k}(H_{o,i} + B_{z,o,j}) \left(\frac{y_{i,j}}{H_{o,i} + B_{z,o,j}} - \frac{y_{i,k}}{H_{o,i} + B_{z,o,k}} \right)} \right\}$$

$$\times \left[\frac{\partial(y_{i,j} - y_{i,k})}{\partial \theta} d\theta + \frac{\partial(y_{i,j} - y_{i,k})}{\partial \varphi} d\varphi + \frac{\partial(y_{i,j} - y_{i,k})}{\partial \tau} d\tau \right]$$

which is more readily adaptable to the computer.

The partials of $a'_{i,j}$, $b'_{i,j}$, and $f'_{i,j}$ are found from equations (9) to be

$$\frac{\partial a'_{i,j}}{\partial \theta} = (b_{i,j} \cos \theta - a_{i,j} \sin \theta) \cos \varphi$$

$$\frac{\partial a'_{i,j}}{\partial \varphi} = f \cos \varphi - (a_{i,j} \cos \theta + b_{i,j} \sin \theta) \sin \varphi$$

$$\frac{\partial a'_{i,j}}{\partial \tau} = 0$$

APPENDIX

$$\frac{\partial b'_{i,j}}{\partial \theta} = -\left(a_{i,j} \cos \theta + b_{i,j} \sin \theta\right)\cos \tau + \left(b_{i,j} \cos \theta - a_{i,j} \sin \theta\right)\sin \varphi \sin \tau$$

$$\frac{\partial b'_{i,j}}{\partial \varphi} = \left[f \sin \varphi + \left(a_{i,j} \cos \theta + b_{i,j} \sin \theta\right)\cos \varphi\right]\sin \tau$$

$$\frac{\partial b'_{i,j}}{\partial \tau} = -\left\{\left(b_{i,j} \cos \theta - a_{i,j} \sin \theta\right)\sin \tau + \left[f \cos \theta - \left(a_{i,j} \cos \theta + b_{i,j} \sin \theta\right)\sin \varphi\right]\cos \tau\right\}$$

$$\frac{\partial f'_{i,j}}{\partial \theta} = \left(b_{i,j} \cos \theta - a_{i,j} \sin \theta\right)\sin \varphi \cos \tau + \left(b_{i,j} \sin \theta + a_{i,j} \cos \theta\right)\sin \tau$$

$$\frac{\partial f'_{i,j}}{\partial \varphi} = \left[f \sin \varphi + \left(a_{i,j} \cos \theta + b_{i,j} \sin \theta\right)\cos \varphi\right]\cos \tau$$

$$\frac{\partial f'_{i,j}}{\partial \tau} = \left[f \cos \varphi - \left(a_{i,j} \cos \theta + b_{i,j} \sin \theta\right)\sin \varphi\right]\sin \tau - \left(b_{i,j} \cos \theta - a_{i,j} \sin \theta\right)\cos \tau$$

with similar expressions of $a'_{i,k}$, $b'_{i,k}$, and $f'_{i,k}$.

REFERENCES

1. Army Map Serv.; and Aeronaut. Chart Inform. Center: Department of Defense Selenodetic Control System 1966. Tech. Rep. No. 1, Def. Intel. Agency, Jan. 1957. (Available from DDC as AD 648067.)

2. The Boeing Company: Lunar Orbiter I – Photographic Mission Summary. NASA CR-782, 1967.

3. Dyer, John P.: Lunar Orbiter Photo Site Accuracy Analysis. Final Report – Error Analysis. NASA CR-66734-3, 1969.

4. Osborn, Roger T.: An Automated Procedure for Producing Contour Charts. IM No. 67-4, U.S. Naval Oceanographic Office, Feb. 1967. (Available from DDC as AD 807617.)

5. Compton, Harold R.; and Wells, William R.: Determination of Lunar Equatorial Radius Using V/H Sensor Data From Lunar Orbiter I. NASA TN D-5231, 1969.

6. Sjogren, William J.; Trask, Donald W.; Vegos, Charles J.; and Wollenhaupt, Wilbur R.: Physical Constants as Determined From Radio Tracking of the Ranger Lunar Probes. Space Flight Mechanics Specialist Symposium, Vol. 11, Maurice L. Anthony, ed., Amer. Astronaut. Soc., 1967, pp. 137-154.

TABLE I.- SITE LOCATIONS AND THE ESTIMATED CAMERA ATTITUDES

Site	Number of features identified	Mean location, deg		Spacecraft state						Estimated camera attitude, radians		
				Position, km			Velocity, m/sec					
		Latitude	Longitude	x	y	z	$\dot{x}$	$\dot{y}$	$\dot{z}$	Swing	Tilt	Roll
I P-1	178	-0.88651288	41.9056644	1334.3855	1196.5620	-27.0379	-1.2372814	1.4006208	-0.3970547	0.00292505	-0.00025237	
I P-2	358	.06228847	35.5485085	1458.8553	1040.8279	2.1092	-1.1003737	1.5106498	-.3984953	.00725908	.00906537	
I P-5	269	.19111405	-1.4667120	1788.6865	-48.4444	3.6554	.0152789	1.8681966	-.4135784	.00361085	.01473142	
I P-7	200	-3.30235474	-22.0999532	1652.1733	-676.2792	-101.2629	.7580113	1.7109278	-.3827314	.01971714	-.02990051	
I P-8.1	184	-3.12162703	-36.4792208	1433.7319	-1063.9228	-98.1348	1.1493975	1.4770890	-.3806640	.00416727	-.00442459	
I P-9.2B	495	-2.40423556	-43.2918948	1295.8572	-1226.0461	-79.9958	1.3017246	1.3464873	-.3835443			
A										.00409131	.00245722	0.00292073
B										.00765435	-.00621596	-.00013686

TABLE II.- COMPARISON OF RADII

Site	Point	Latitude, deg	Longitude, deg	Radius, km	
				Photo analysis (a)	V/H sensor (b)
I P-1	1	-0.58	40.55	1736.02	1735.44
	2	-.88	41.97	1735.52	1735.18
I P-2	1	0.37	34.08	1734.82	1735.35
	2	.30	35.49	1735.82	1736.20
	3	-.23	36.91	1735.60	1736.09
I P-5	1	0.42	-2.92	1735.76	1736.78
	2	.11	-1.51	1736.13	1736.77
I P-7	1	-3.12	-22.86	1736.50	1736.76
	2	-3.41	-21.44	1735.92	1736.78
I P-8.1	1	-3.23	-36.14	1735.31	1735.88
I P-9.2A	1	-2.08	-43.81	1735.31	1735.60
	2	-2.37	-42.39	1735.26	1735.76
I P-9.2B	3	-2.35	-44.47	1735.65	1735.67
	4	-2.64	-43.06	1735.42	1735.74

[a]Computations have an estimated uncertainty of ±0.2 km.

[b]Computations have an estimated uncertainty of ±0.7 km.

TABLE III.- RADII DERIVED FROM RANGER IMPACT DATA

Mission designation	Impact point		Local radius
	Latitude	Longitude	
Ranger VI	9.3	21.4	1735.3
Ranger VII	-10.7	-20.7	1735.5
Ranger VIII	2.7	-24.8	1735.2
Ranger IX	-12.9	-2.4	1735.7

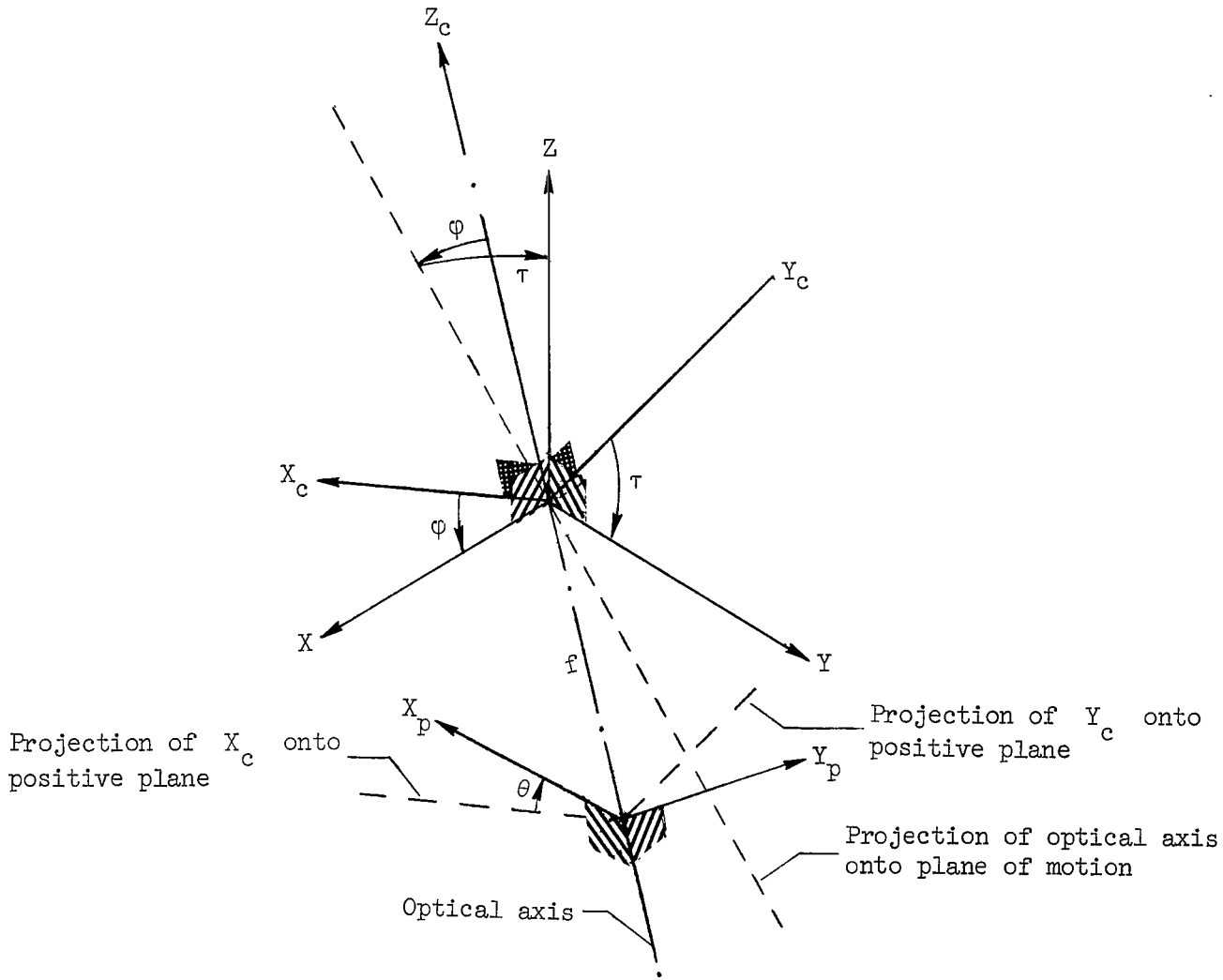

Figure 1.- Components of the camera attitude defined relative to the orbital plane and the spacecraft radius vector.

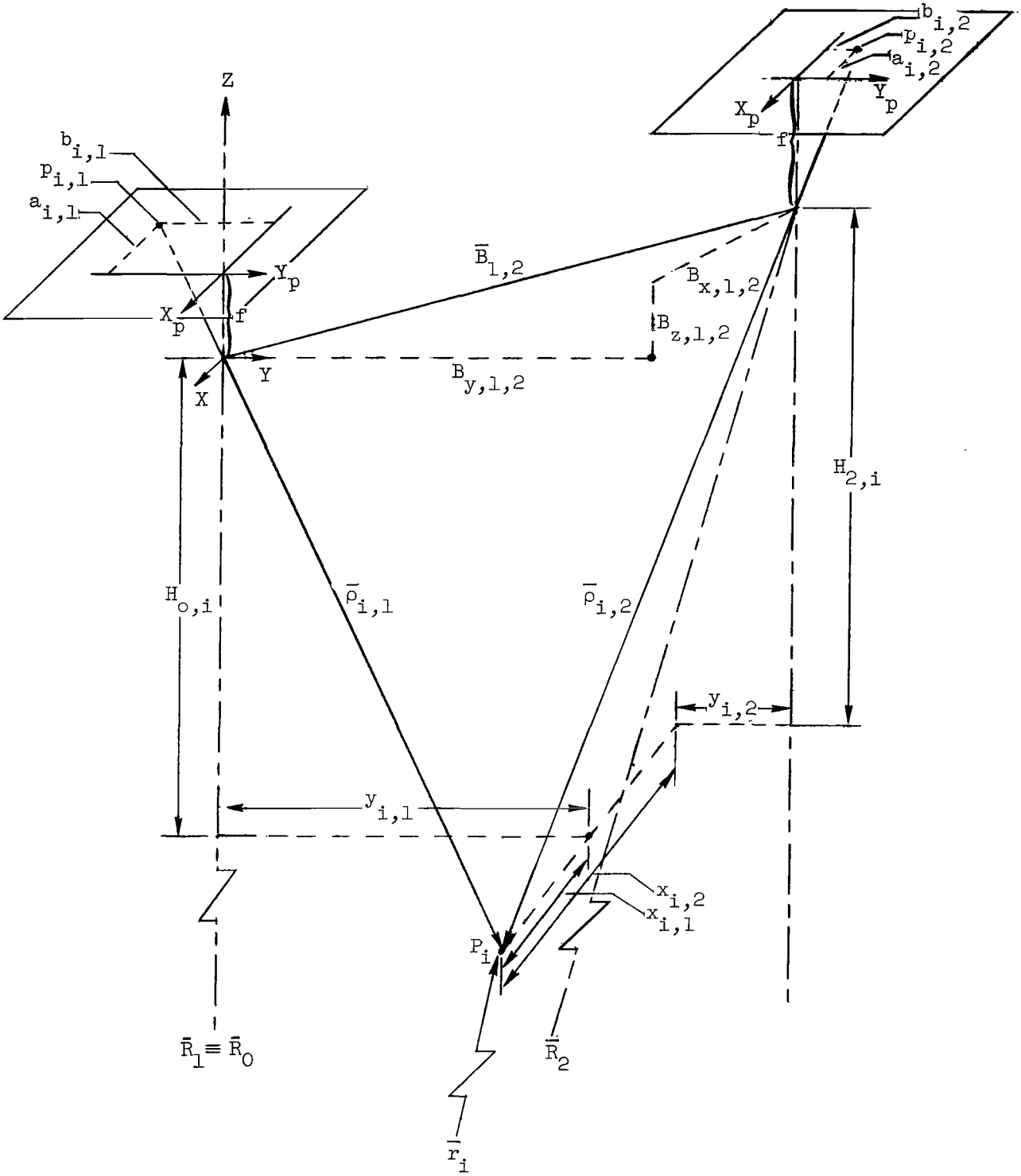

Figure 2.- The geometry of the projection of the image of a point through a normally oriented camera lens at two positions of the camera.

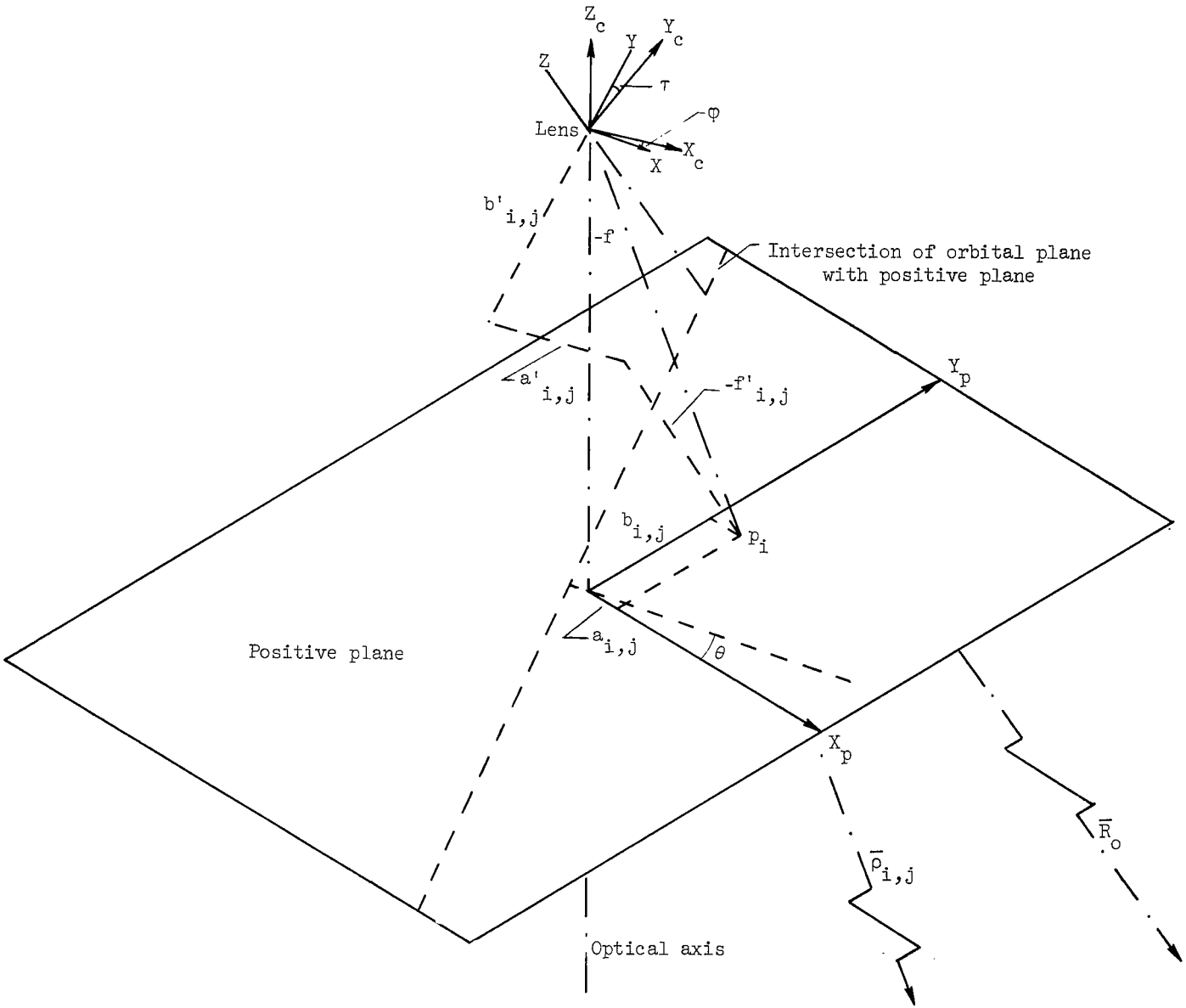

Figure 3.- The geometry of transforming image coordinates in the photographic coordinate system to their equivalent in the X,Y,Z system.

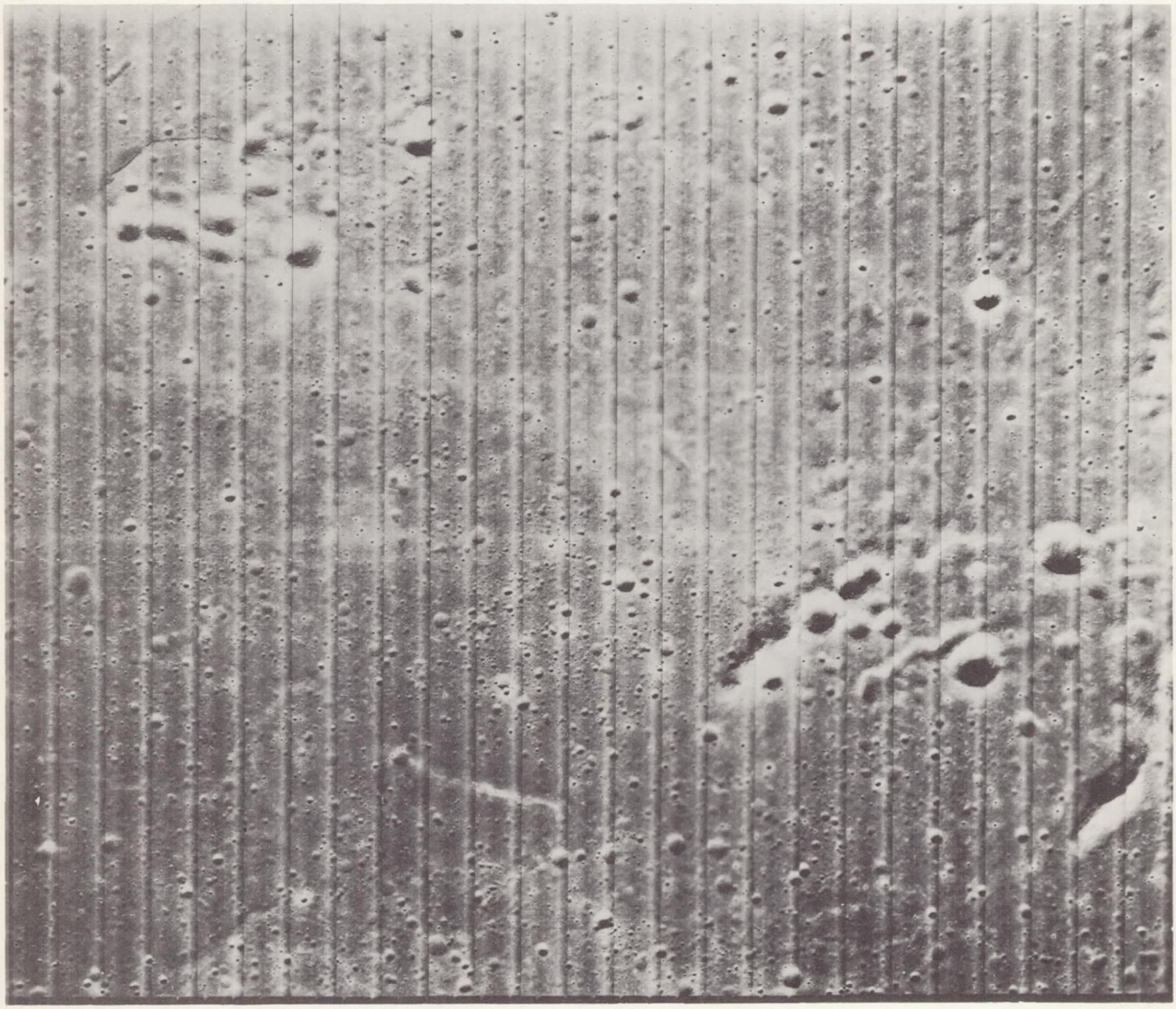

Figure 4.- A typical Lunar Orbiter photograph. L-69-1307

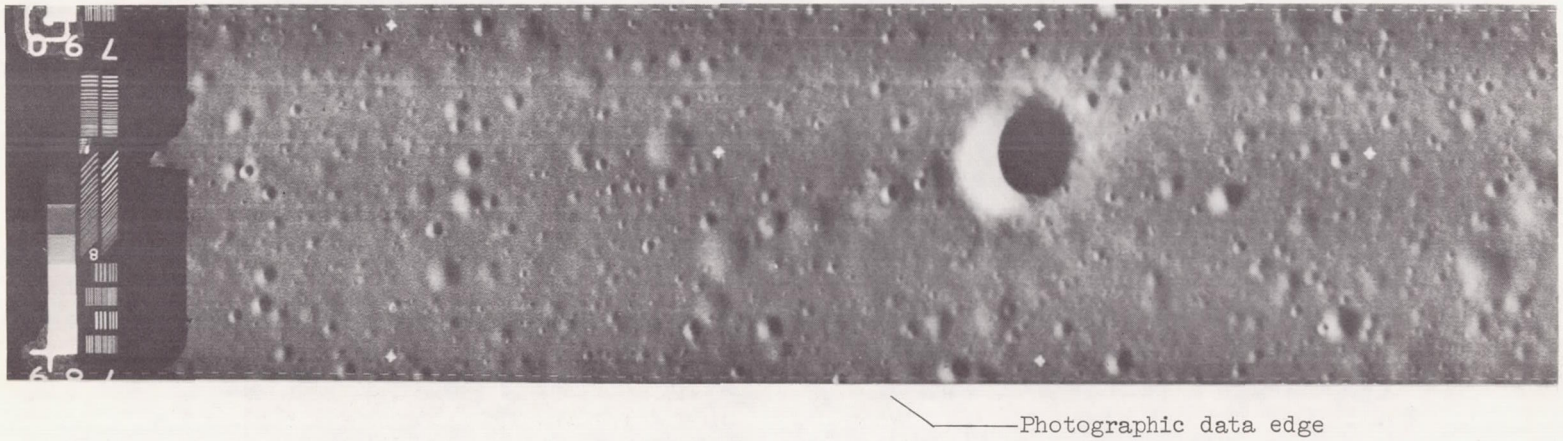

Figure 5.- An enlarged portion of a typical framelet with the leading edges of two consecutive gray scales shown. L-69-1308

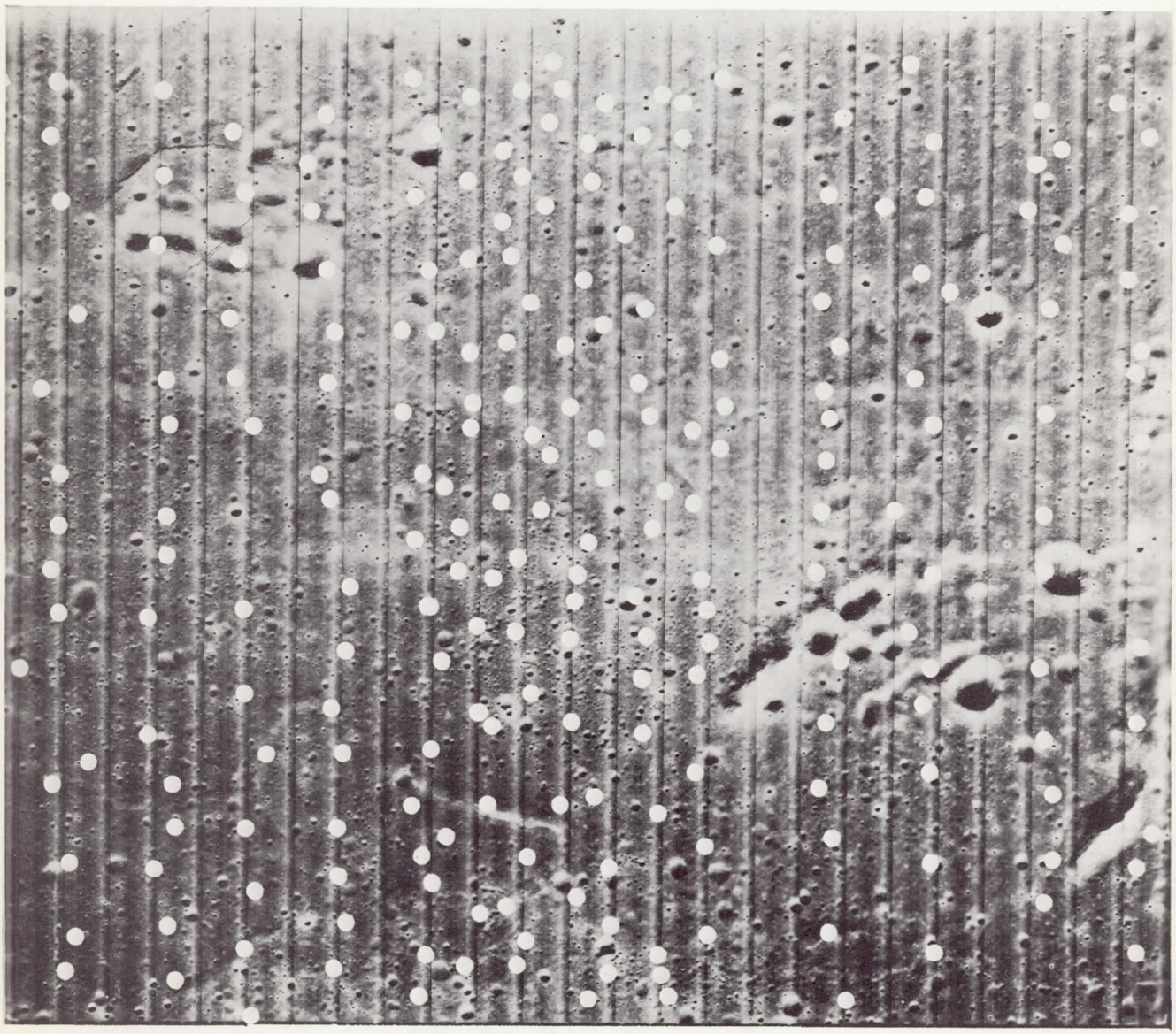

Figure 6.- An example of the desired distribution of identified features on a composite. L-69-1309

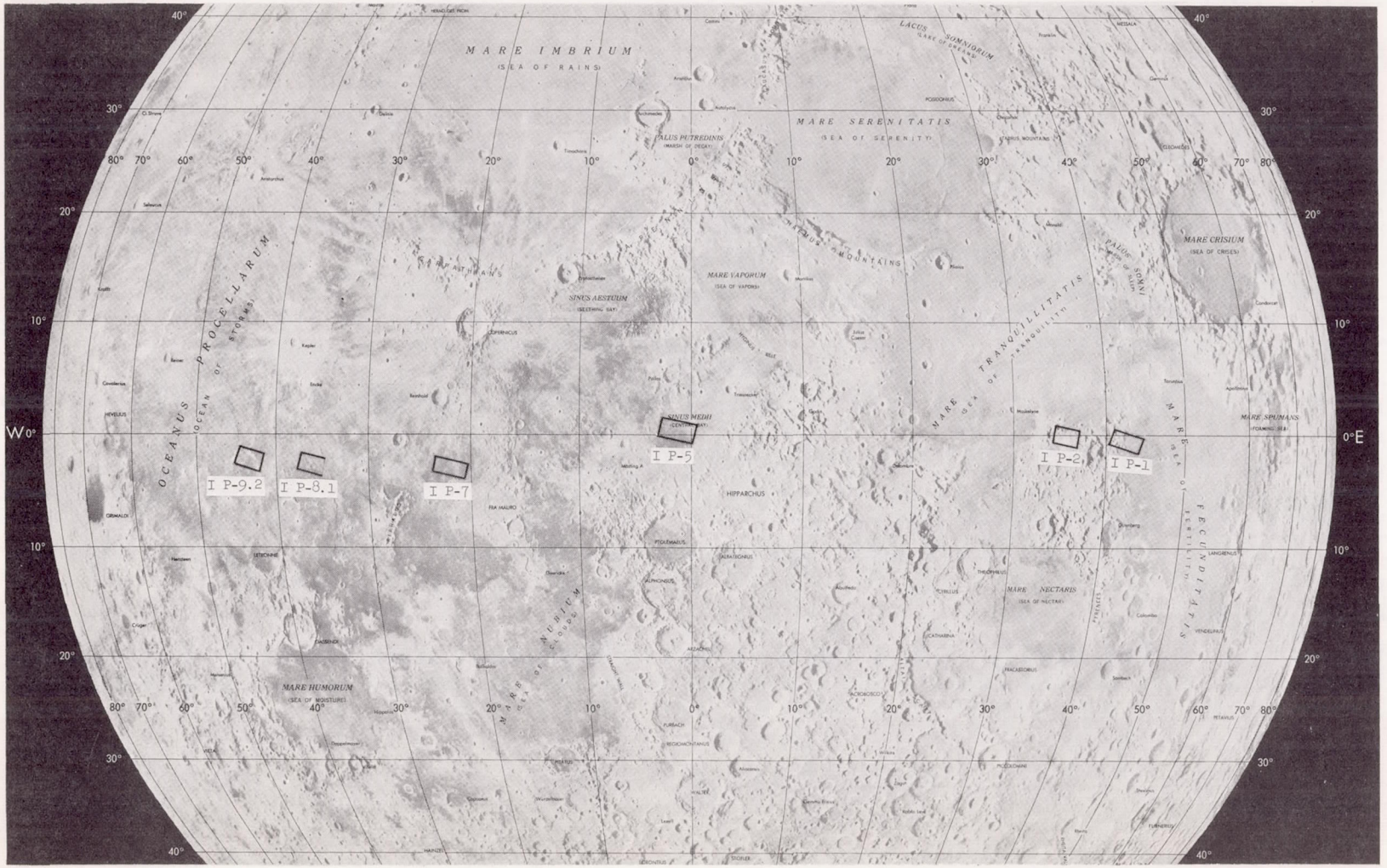

Figure 7.- Approximate locations of the Lunar Orbiter I primary sites processed.

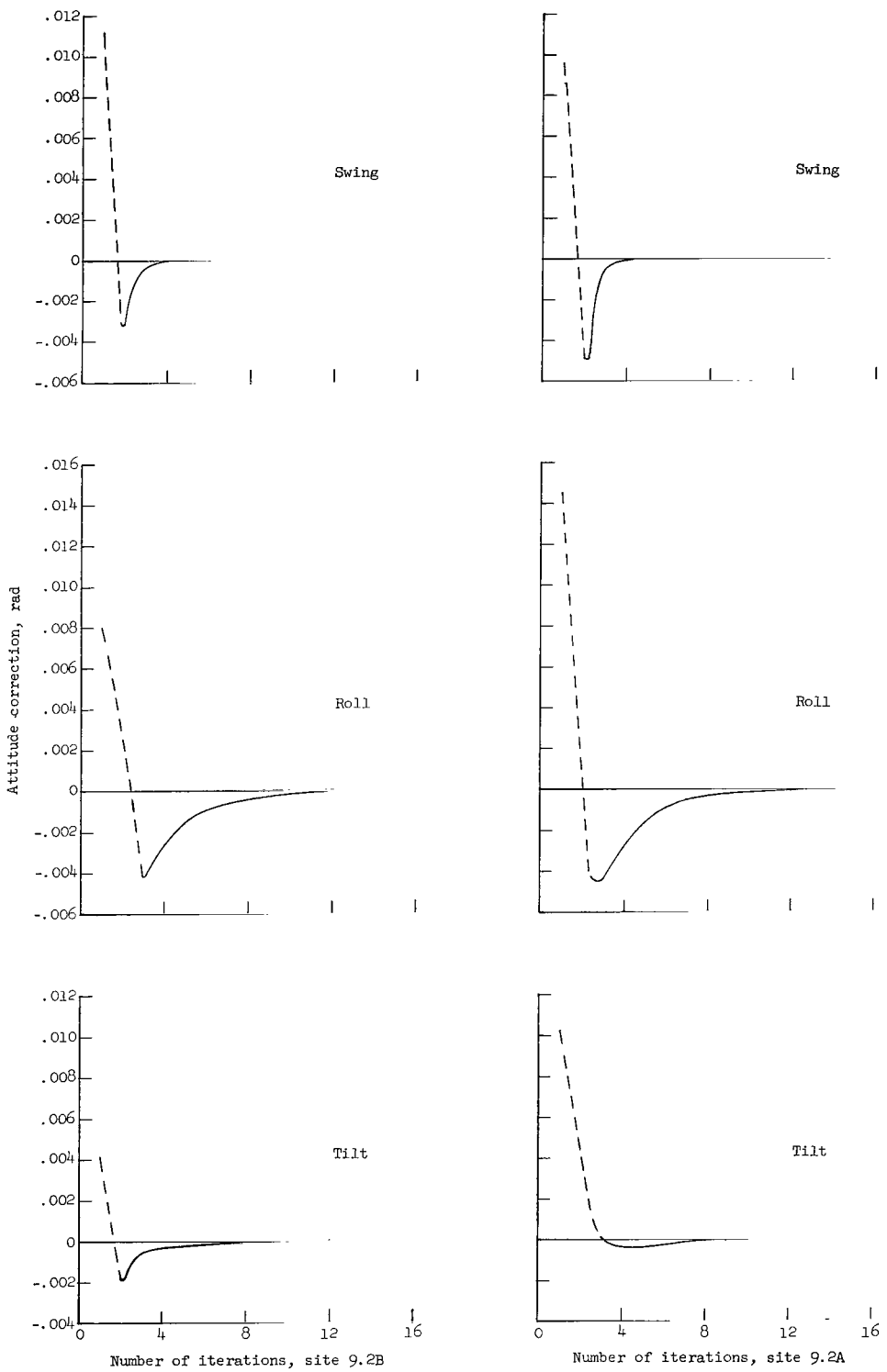

Figure 8.- Convergence of the components of the camera attitude for sites 9.2A and 9.2B when solved simultaneously.

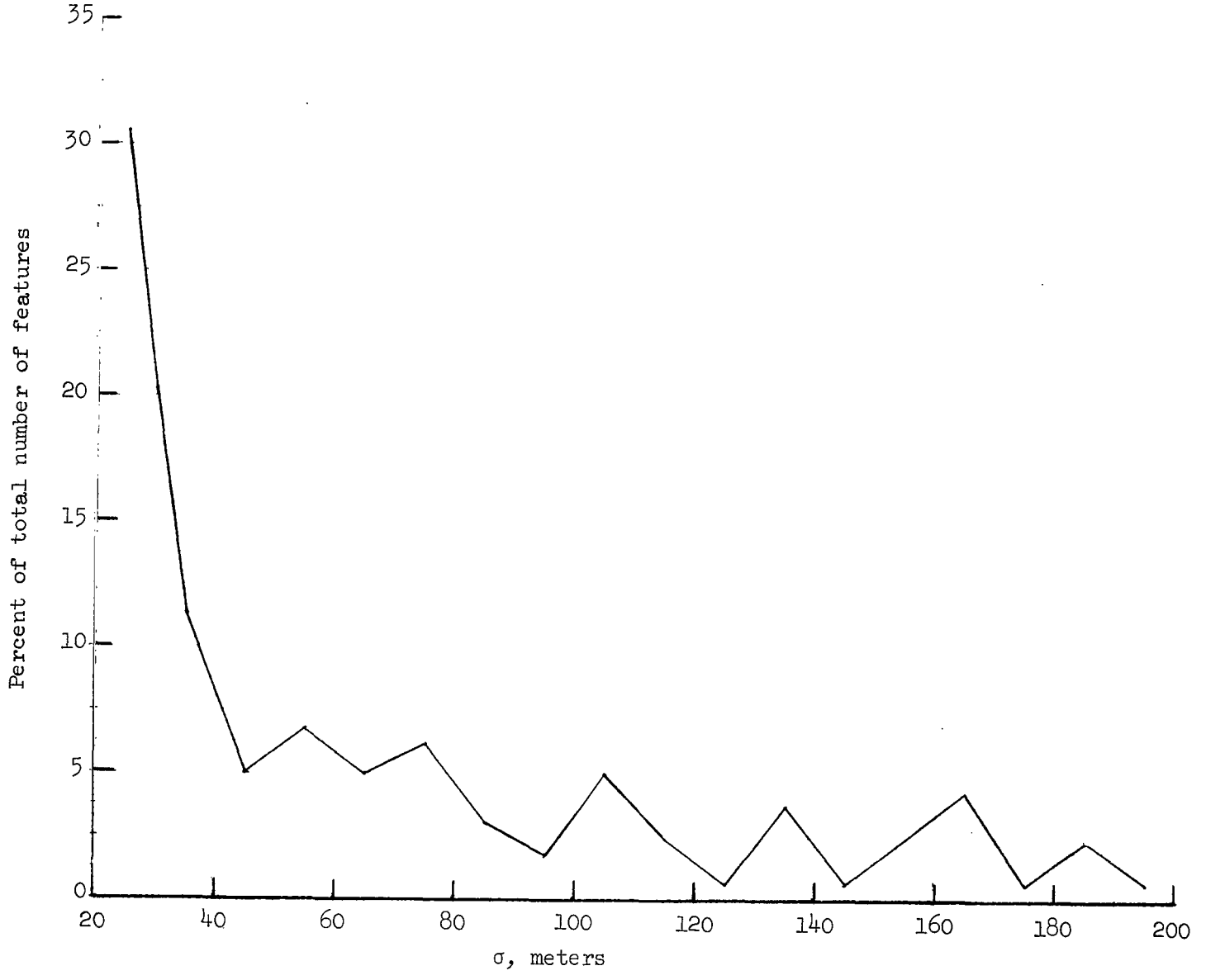

Figure 9.- The percent of the total number of features whose standard deviation of the mean lie between (σ ± 5) meters.

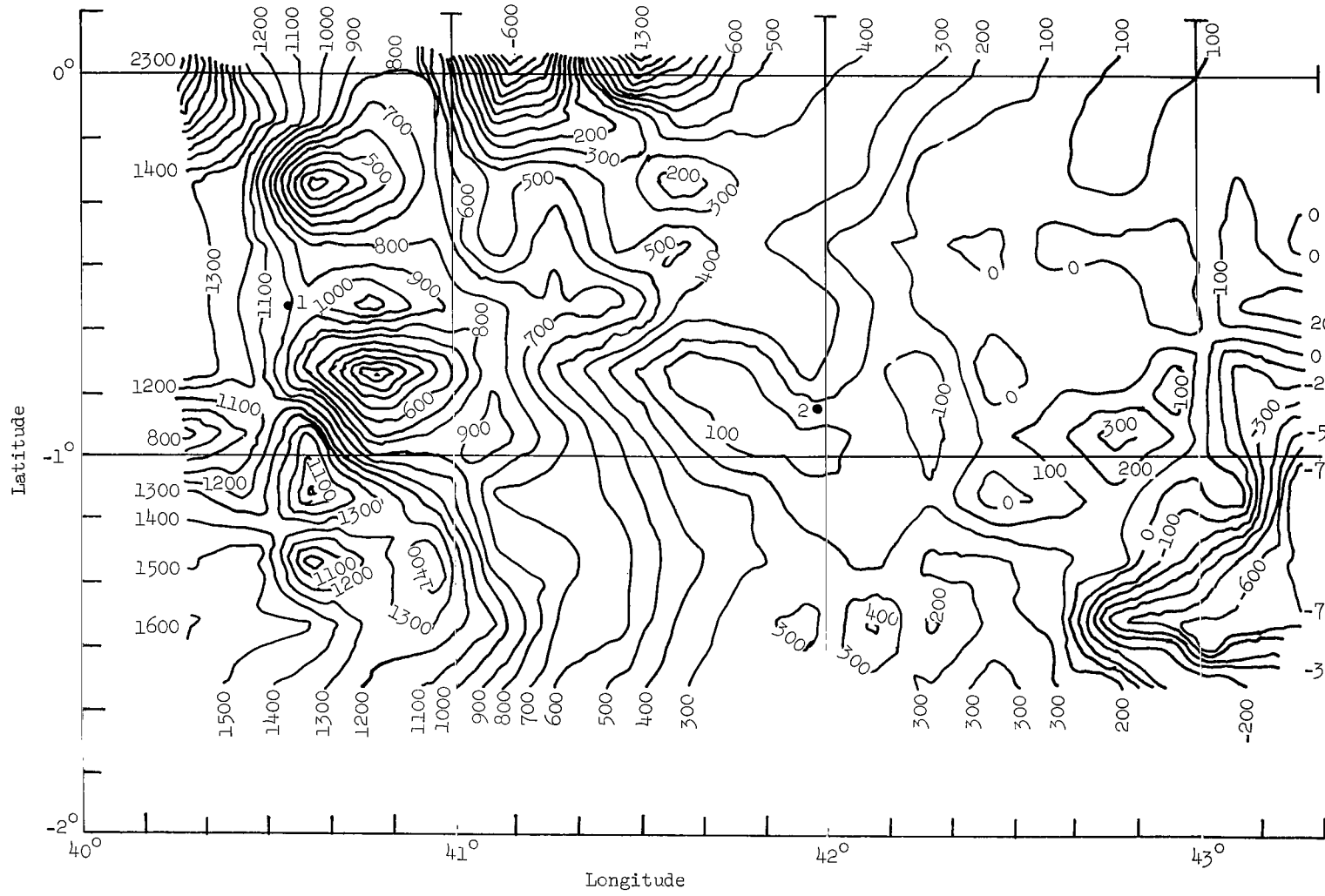

Figure 10.- A computer-generated contour chart of site I P-1. Scale: 10 min ≡ 5047 m.

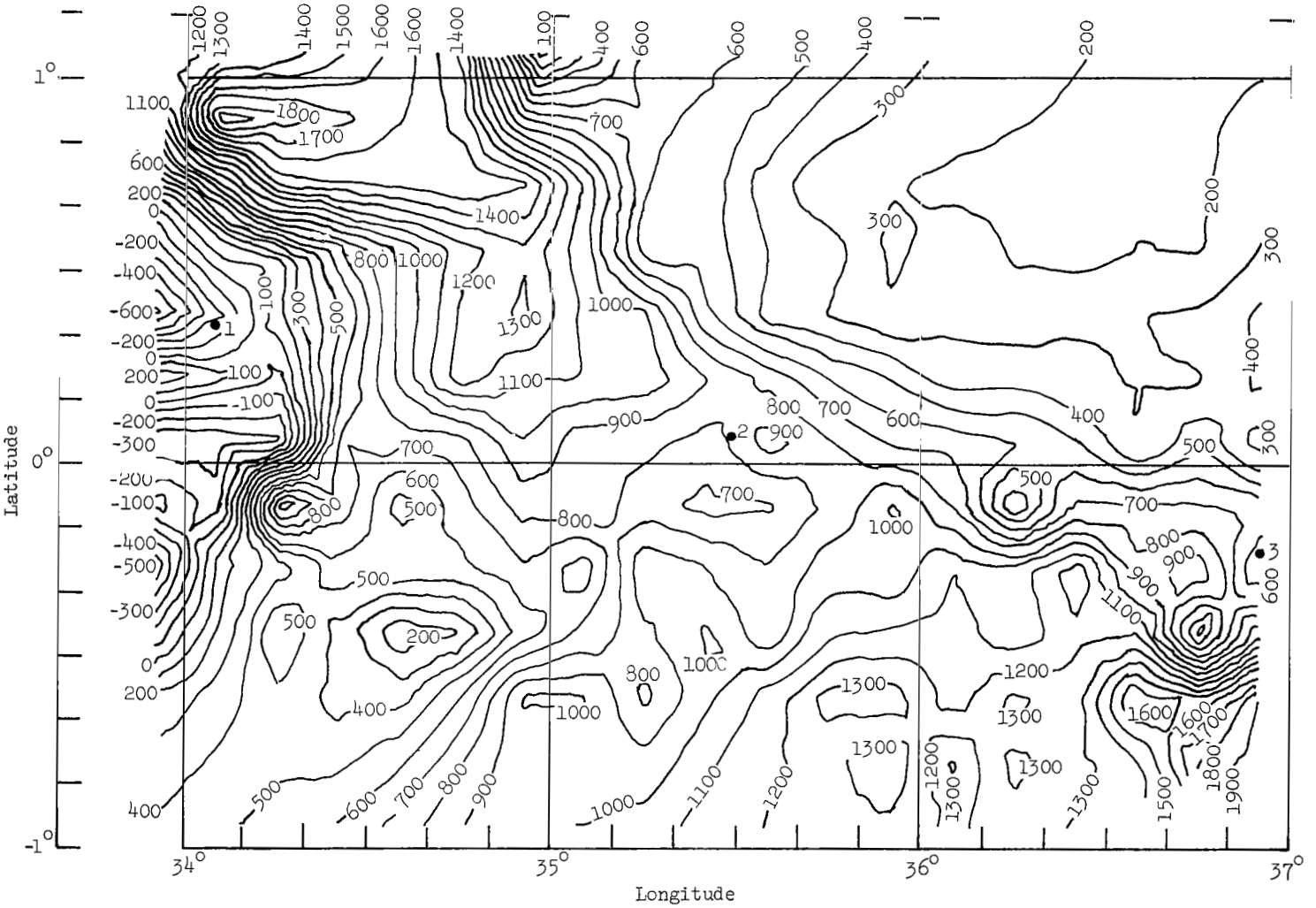

Figure 11.- A computer-generated contour chart of site I P-2. Scale: 10 min ≡ 5047 m.

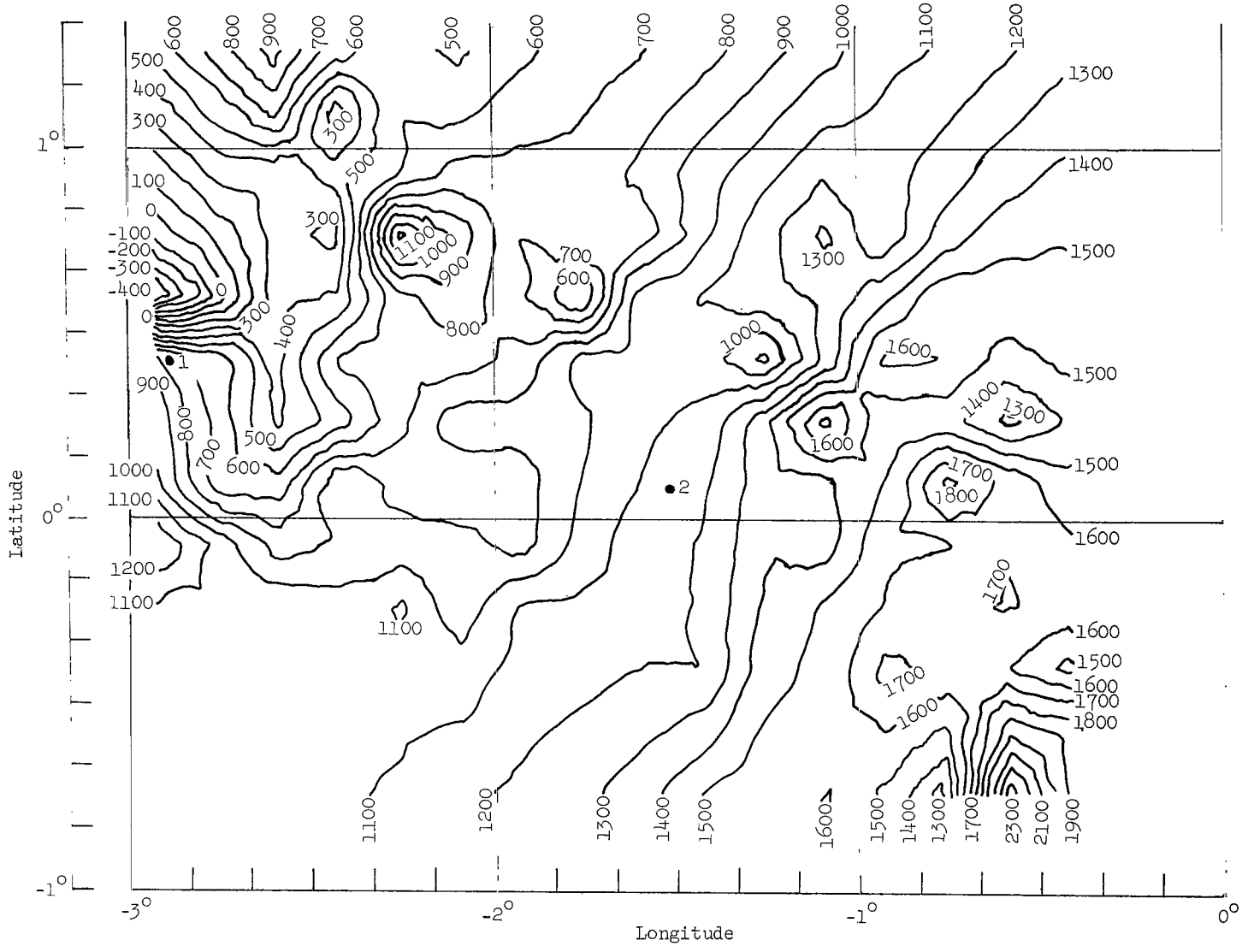

Figure 12.- A computer-generated contour chart of site I P-5. Scale: 10 min ≡ 5047 m.

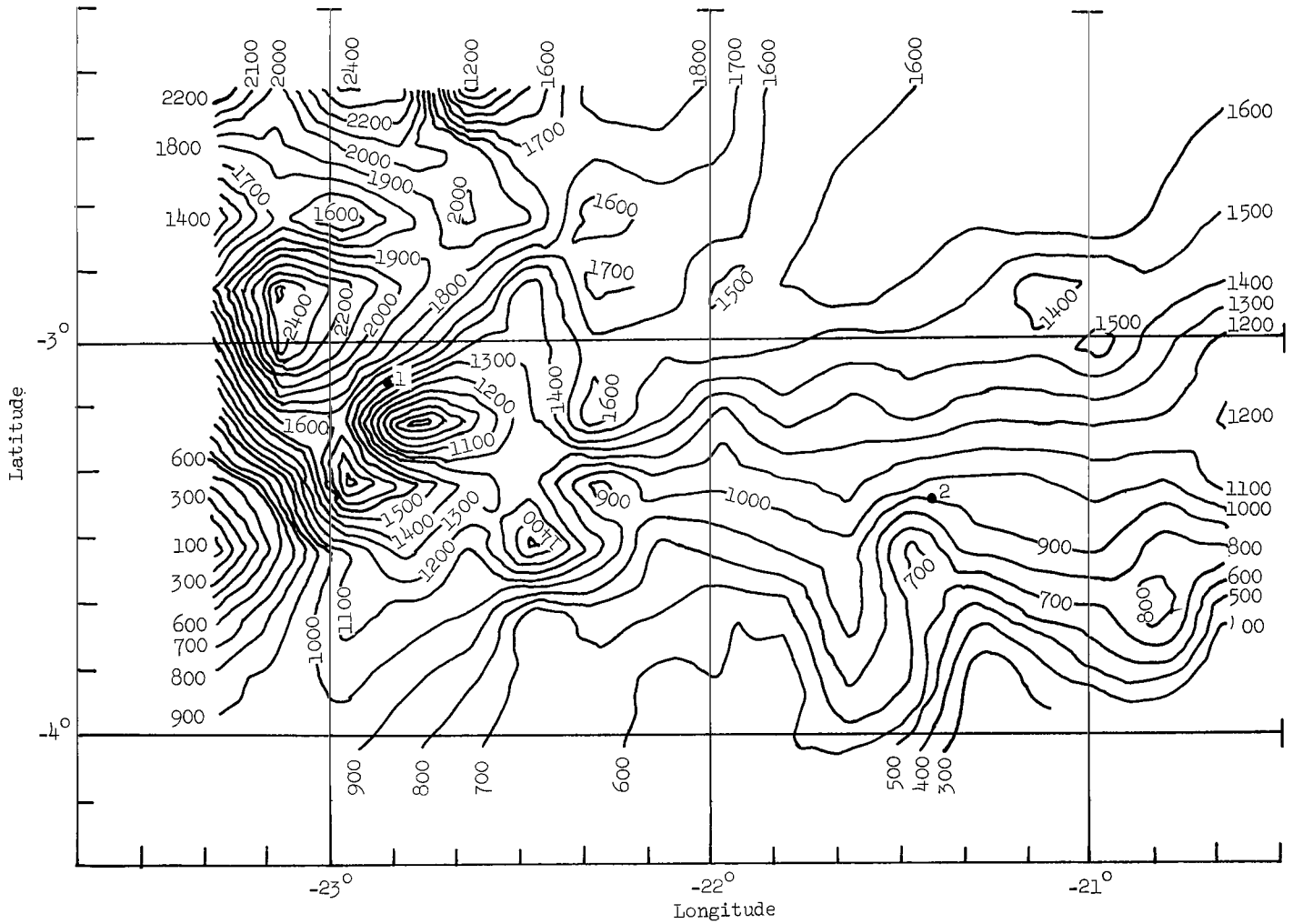

Figure 13.- A computer-generated contour chart of site I P-7. Scale: 10 min ■ 5047 m.

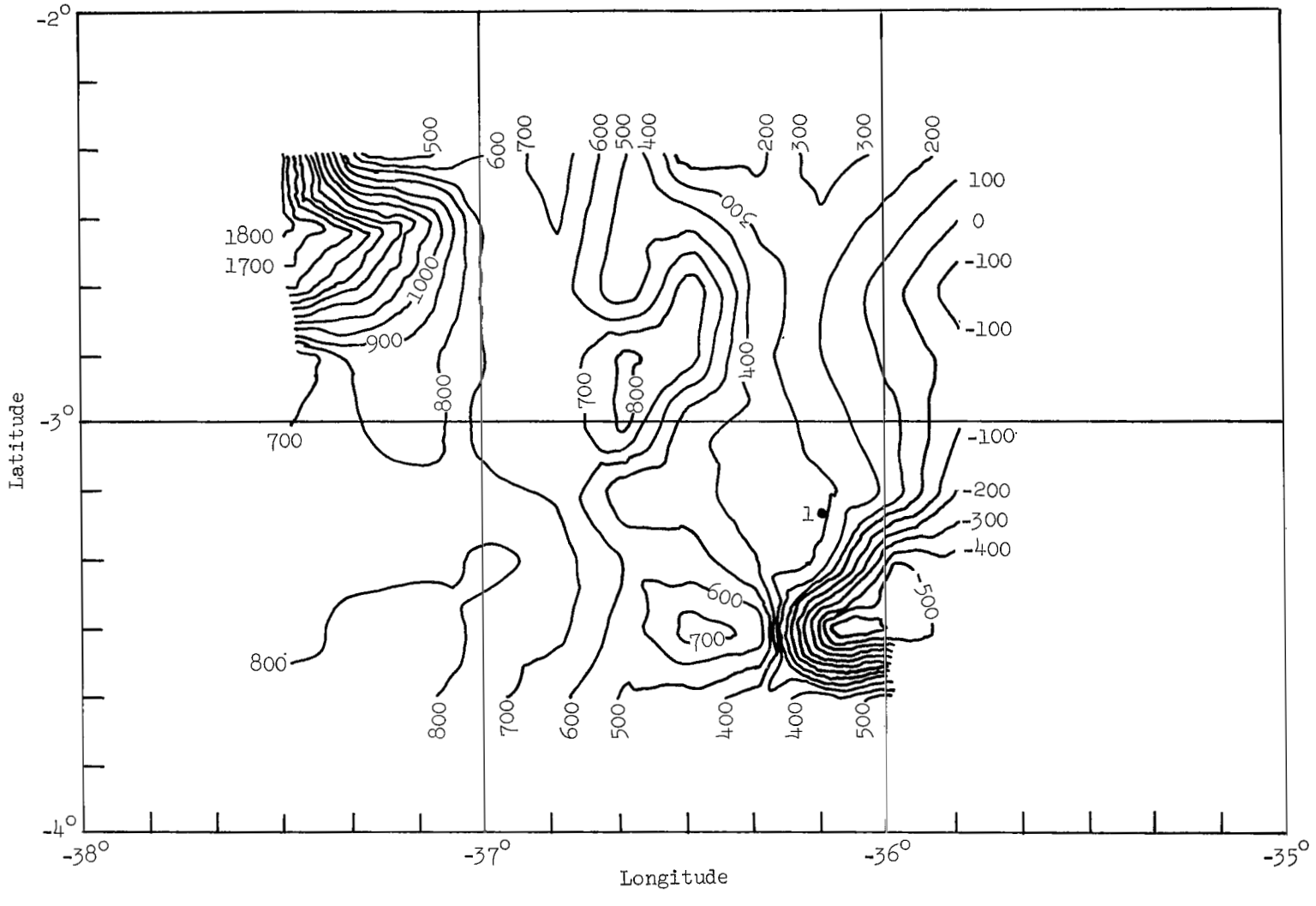

Figure 14.- A computer-generated contour chart of site I P-8.1. Scale: 10 min ≡ 5047 m.

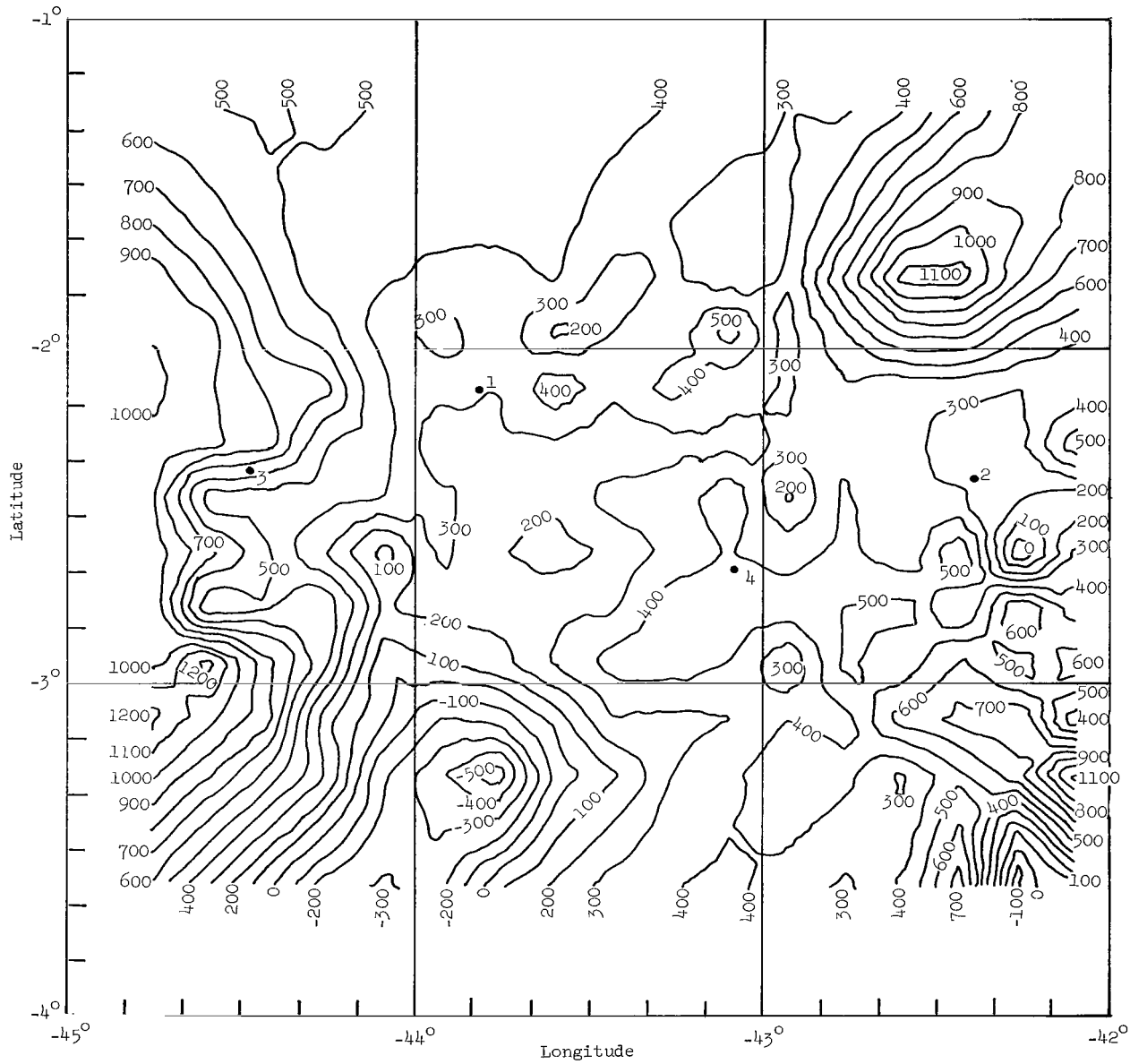

Figure 15.- A computer-generated contour chart of site I P-9.2A and I P-9.2B. Scale: 10 min ≡ 5047 m.

NATIONAL AERONAUTICS AND SPACE ADMINISTRATION
WASHINGTON, D. C. 20546

OFFICIAL BUSINESS

FIRST CLASS MAIL

POSTAGE AND FEES PAID
NATIONAL AERONAUTICS AND
SPACE ADMINISTRATION

POSTMASTER: If Undeliverable (Section 158 Postal Manual) Do Not Return

"The aeronautical and space activities of the United States shall be conducted so as to contribute . . . to the expansion of human knowledge of phenomena in the atmosphere and space. The Administration shall provide for the widest practicable and appropriate dissemination of information concerning its activities and the results thereof."

—NATIONAL AERONAUTICS AND SPACE ACT OF 1958

NASA SCIENTIFIC AND TECHNICAL PUBLICATIONS

TECHNICAL REPORTS: Scientific and technical information considered important, complete, and a lasting contribution to existing knowledge.

TECHNICAL NOTES: Information less broad in scope but nevertheless of importance as a contribution to existing knowledge.

TECHNICAL MEMORANDUMS: Information receiving limited distribution because of preliminary data, security classification, or other reasons.

CONTRACTOR REPORTS: Scientific and technical information generated under a NASA contract or grant and considered an important contribution to existing knowledge.

TECHNICAL TRANSLATIONS: Information published in a foreign language considered to merit NASA distribution in English.

SPECIAL PUBLICATIONS: Information derived from or of value to NASA activities. Publications include conference proceedings, monographs, data compilations, handbooks, sourcebooks, and special bibliographies.

TECHNOLOGY UTILIZATION PUBLICATIONS: Information on technology used by NASA that may be of particular interest in commercial and other non-aerospace applications. Publications include Tech Briefs, Technology Utilization Reports and Notes, and Technology Surveys.

Details on the availability of these publications may be obtained from:

SCIENTIFIC AND TECHNICAL INFORMATION DIVISION

NATIONAL AERONAUTICS AND SPACE ADMINISTRATION

Washington, D.C. 20546